ABSTRACT

Title of Thesis: Material Growth of InGaAs/InAlAs Superlattices for
Quantum Cascade Laser Application

Jiun-Yun Li
Master of Science, 2007

Thesis Directed By: Professor Julius Goldhar
Department of Electrical and Computer Engineering
University of Maryland, College Park
Professor Fow-Sen Choa (Co-Advisor)
Department of Computer Science and Electrical Engineering
University of Maryland, Baltimore County

Quantum Cascade Lasers (QCLs) have rapidly advanced to a leading position among infrared light sources, and are being used in a number of chemical sensing and spectroscopic applications. Most of these devices are grown by molecular beam epitaxy (MBE) except for some of those grown by metalorganic chemical vapor deposition (MOCVD). This thesis investigates the material growth of near-infrared (NIR) QCLs of InGaAs/InAlAs lattice-matched system using MOCVD. The effects of various growth parameters were understood by detailed study on the material properties of InGaAs and InAlAs. Also, in-depth study on InGaAs/InAlAs superlattices shows that there exists a growth window to optimize their performance. With proper interruption periods of growth between individual layers, the hetero-interfacial defects can be reduced at high growth temperature without surface degradation of constituent layers. Finally, the preliminary study of NIR QCLs with digital alloys insertion was conducted and some QCLs wafers were grown successfully.

MATERIAL GROWTH OF INGAAS/INALAS SUPERLATTICES FOR
QUANTUM CASCADE LASER APPLICATION

By

Jiun-Yun Li

Thesis submitted to the Faculty of the Graduate School of the
University of Maryland, College Park, in partial fulfillment
of the requirements for the degree of
Master of Science
2007

Advisory Committee:
Professor Julius Goldhar, Chair/Academic Advisor
Professor Fow-Sen Choa, Co-Chair/Research Advisor (UMBC)
Professor Christopher C. Davis
Assistant Professor Thomas E. Murphy

Dedication

To my wife, Amy

for her endless love and support.

To my parents and brother,

for their encouragement and love.

Acknowledgements

My sincere appreciation goes to my research advisor, Dr. Fow-Sen Choa, for his patience, thoughtful guidance and full support for my thesis work at the University of Maryland, Baltimore County. His wisdom, knowledge, and experiences led me through the difficulty in the course of my research project of quantum cascade lasers. He has enlightened me on and led me into the field of material growth. Here I give my sincerest thank you to him.

I was so lucky to be advised by Dr. Julius Goldhar at College Park. With his big help, this thesis draft was corrected and modified to become a readable work. I appreciate his help during my graduate study in College Park. I also particularly appreciate the comments and suggestions from Drs. Christopher Davis and Thomas Murphy. Their invaluable suggestions and interests in my thesis work have driven me to continue the work and to realize its importance. I am also thankful to their comments on my draft writing, which is priceless for my career. Thanks for my colleagues Xiaoming Ji and Liwei Cheng for their help as I started to learn the growth, and thanks for the discussion we had together.

Last, I must say thank you to my wife, Amy. As I suffered, she comforted; as I was struggled, she supports; as I was lost, she led me. Without her, this thesis would not be completed. Thank you, my lovely wife.

Table of Contents

List of Figures

Chapter 1

Introduction to Quantum Cascade Lasers

1.1   Overview

Quantum cascade lasers (QCLs), which are based on intersubband transitions, were first proposed at 1971 by Kasarinov and Suris [1] to amplify the light in the intersubband transition by photon-assisted tunneling. Little progress had been made for almost 20 years since the prediction by these two researchers because the population inversion was not easily achieved for the extremely short lifetime of the electrons. In 1994, Faist [2] *et al*. in Bell Lab demonstrated the first quantum cascade lasers with intersubband transitions inside the conduction band by externally applying a high electric field. These lasers were operated at cryogenic temperatures. The electrons within conduction band can be reused to emit multiple numbers of photons, which are proportional to the number of stages (N_p) without recombination with holes. The efficiency and operation temperature were raised by the careful design of the light emitting region (active region) and the injector region which is extremely important for population inversion. The emission wavelength of these lasers can be controlled by adjusting the thickness of the quantum wells, rather than by material's bandgap energy. By using the lattice-matched systems (i.e. InGaAs/InAlAs matched to InP, or GaAs/AlGaAs matched to GaAs), we can design and grow any combination of well and barrier layers to emit photons with desired wavelengths.

1.2 Basic Concepts

Compared to traditional semiconductor lasers, there are two fundamental features for QCLs: unipolarity and cascading process (Fig. 1-1). The former is extremely important and fundamentally different from the conventional interband lasers in that the electrons are the only carriers (at least so far) involved in the photon emission process. Unlike the interband lasers utilizing electron-hole pair recombination for photon emission, QCLs employ the transition of electrons from the initial to final states within the conduction band, which have the same curvatures in the reciprocal space. Thus, the joint density of states is very sharp, which is close to atomic transitions, resulting in the gain spectrum with narrow linewidth (Fig. 1-2).
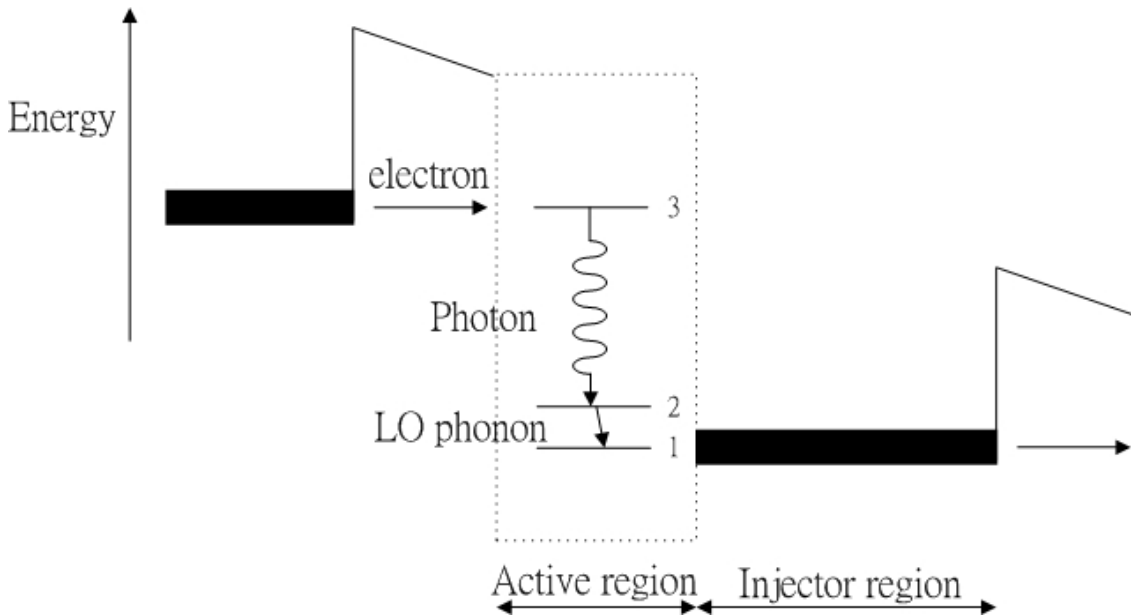
Fig. 1-1: Operation principle of a quantum cascade laser structure within conduction band. Only electrons involve light emission and each period consists of an active region and an injector region.
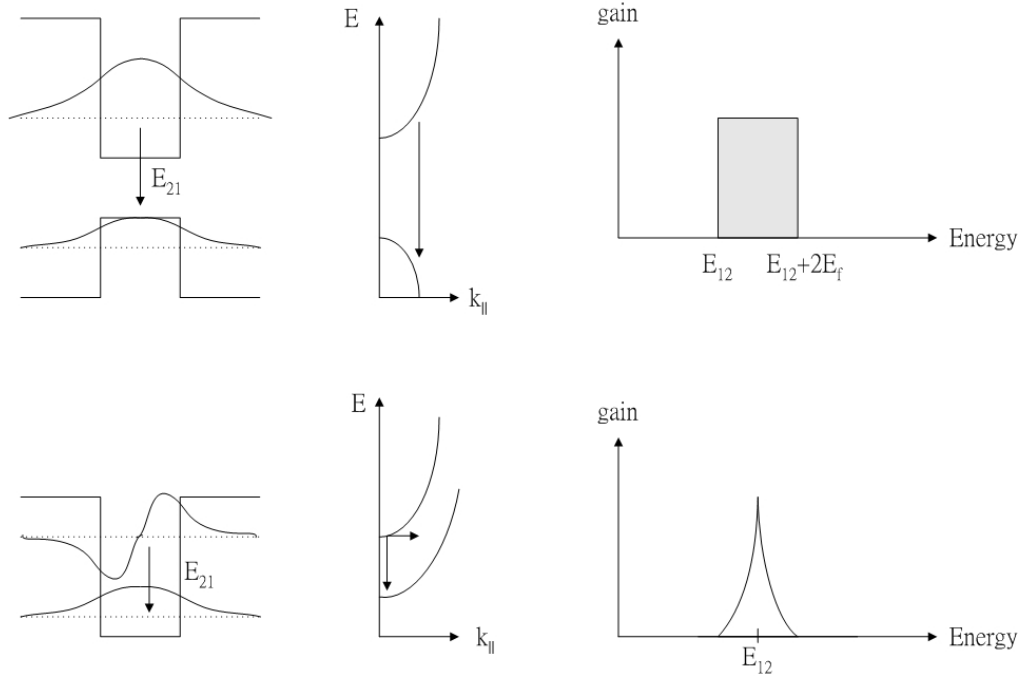
Fig. 1-2: Interband transition (top) vs. intersubband transition (bottom). Left: potential profile in real space; Middle: dispersion of the electronic intersubbands in the plane; Right: joint density of states.

The second feature of QCLs, cascading process, is also of crucial importance. The carriers in traditional semiconductor lasers are supplied by optical or electrical pumping with each carrier only used once. In contrast, QCLs utilize electrons as carriers and reuse them inside the whole structure before they exit. At each stage, each electron, in principle, can emit one photon and thus we can increase the number of stages to increase laser output power and efficiency. Indeed, the high efficiency and high power QCLs have been demonstrated [3]. The study in the effect of stage number on the device performance was discussed in detail in [4].

The basic principles of QCL operation is as follows. Fig. 1-3 shows the unit structure of mid-IR quantum cascade lasers under an external electric field. The injector region is sandwiched by two active regions. For InP-based system, the well

and barrier materials are $In_{0.53}Ga_{0.47}As$ and $In_{0.52}Al_{0.48}As$ lattice-matched to the InP substrate. We can readily solve Schrödinger's equation for this potential set and tune the subband levels to the right positions for specific wavelengths. Under this electric field (10 ~ 100 kV/cm), electrons are injected from the ground state G of the previous injector into the level 3, the upper laser state, of the active region. The scattering rates of electrons from level 3 into the lower levels 2 and 1 are very high due to the LO phonon emission. With the injector regions, the carriers can be extracted efficiently from the lower laser state into the ground state of the injector region. Repeating this process, an electron will emit multiple photons within this cascading structure resulting in high output powers.
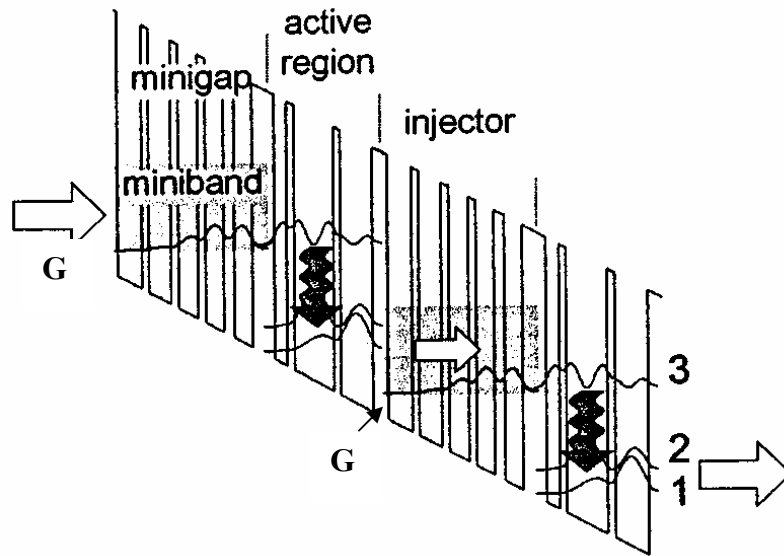
Fig. 1-3:   Quantum cascade laser structure with two repeated units consisting of active and injector regions. The moduli of the wavefunctions are also shown with the level 3 of upper laser lever, level 2 of the lower laser level, and level G of ground state in injector regions. [5].

Because of the longer wavelength of QCLs compared to conventional semiconductor lasers, free carrier absorption loss from doped semiconductors

becomes critical. In addition, the optical loss from the overlap of the optical field with the metallic contact layer needs to be minimized for high-performance QCLs. The first QCL in 1994 used InAlAs as the cladding layers due to its low refractive index ~ 3.20. The core region, which includes active and injector regions, usually has 500 stacking layers consisting of alternative InGaAs and InAlAs layers with total thickness about 1.5 to $2.5\,\mu$m. The average refractive index in this region can be calculated according to the volume fraction of these two constituent materials and is often ~3.35, which is clearly higher than the cladding layers [6]. The confinement factor with typical N_p~30 is usually ~ 0.5. To reduce the optical loss, the cladding layers are usually doped with low concentration to $5\times10^{16}\,cm^{-3}$ and the separate confinement heterostructures (SCH) are implemented with InGaAs of high refractive index to increase the optical confinement factors. In later designs, the InAlAs cladding layers were replaced by InP because it has a lower refractive index ~ 3.10 and higher thermal conductivity for better heat treatment, which is a critical step for the device performance [6].

So far, the emission wavelength of QCLs has been extended from the near infrared (NIR) to terahertz (THz) regimes. While the longest demonstrated wavelength is 1.6 ~ 1.8 THz with GaAs/Al$_{0.1}$Ga$_{0.9}$As system at 80 K under continuous-wave (cw) operation [7], the shortest wavelength has been extended to $3\,\mu$m with In$_{0.53}$Ga$_{0.47}$As/AlAs$_{0.56}$Sb$_{0.44}$ system at 300 K under pulsed operation [8]. The highest output power of short-wavelength QCL ($4.6\,\mu$m) under cw operation at room-temperature is demonstrated by the Northwestern group with 100 mW and the highest operation temperature was raised to 105°C. All of these state-of-the-art QCLs

so far have been grown by molecular beam epitaxy (MBE), but for industry, metalorganic chemical vapor deposition (MOCVD) is preferable for mass production. As a result, attempts have been made to grow QCLs by MOCVD. Until now, there are only three groups successfully reporting the growth of QCLs by MOCVD [9]-[11]. More effort is still required for MOCVD growers to develop more advanced techniques to compete with MBE. In our group, interest in QCLs growth was initiated in 2006. A study of the optimization of material growth was performed and will be discussed in this thesis.

1.3   Applications

QCLs have become a candidate for applications that require mid-infrared (MIR) wavelength sources such as trace-gas sensing. As a result of molecular rotation-vibration transitions, most trace gases of importance have absorption bands in this wavelength range. Therefore, narrow-linewidth, tunable, and single-mode laser devices with high power have been thought to be the best solution to detect these trace gases by a measurement technique called "tunable infrared laser diode absorption spectroscopy (TILDAS) [12] which has advantage of compactness, robustness, portability, and high sensitivity. Soon after distributed feedback QCLs were invented [13], they have been put into action in sensing application [14].

Moreover, ultrafast intersubband scattering (~ 1ps) has major implications for high-speed operation characteristics of QCLs. Gain-switching, and active and passive mode locking were also demonstrated with repetition rates of 100 MHz to 10 GHz [6].

In the future, these pulsed mid-infrared sources may be useful for time-resolved spectroscopy, as well as in high-speed infrared wireless communication systems.

1.4   Motivation and Organization

Up to now, most QCLs have been grown by MBE, which has been considered the most powerful technique to provide atomic-scale interfacial quality. However, the extremely low growth rate, which is believed to be its major advantage, to grow sharp interfaces over MOCVD, takes much longer time to grow the whole QCL structure (> 5 hr). Besides, difficulty in growing phosphorous-related compound materials has restricted its use for the growth of cladding InP layers. Thus, InAlAs was used in the first QCLs as its cladding layer, whose material quality and thermal conductivity are poorer and the confinement effect is weaker than InP. For thick InP cladding layers, MOCVD is thought to be the best candidate. Consequently, despite its higher growth rate (7 Å/s), mid-infrared QCLs with room-temperature operation have been demonstrated by MOCVD recently [9]-[11]. With the interruption between individual layers by purging the group-V hydride gas, interface roughness can be reduced and the device performance is comparable to those grown by MBE. This pioneering work encouraged us to exploit the possibility of growing NIR QCLs that have only been grown by MBE previously. With a new scheme proposed by the Fraunhofer group [15] utilizing the binary alloys InAs and AlAs inserted into the typical matched InGaAs/InAlAs system, the emission wavelength can be extended to the NIR regime. Though this structure still requires more effort to prove its robustness and flexibility,

the ease of growing the binary materials and high-quality Al-containing materials are attractive for MOCVD growers [16].

In this thesis, I will focus on the material growth of InGaAs and InAlAs. Before the discussion of InGaAs and InAlAs materials, the principles of MOCVD are introduced in Chapter 2, which will discuss the mechanism of epitaxy and the factors affecting the growth. Chapter 3 discusses the growth, characterization, and the lattice mismatch conditions of InGaAs and InAlAs. In Chapter 4, the growth conditions of InGaAs and InAlAs are optimized to prepare InGaAs/InAlAs superlattices. The extension of the growth window to higher growth temperature by increasing growth rate and interruption period is also demonstrated in this chapter. Finally, Chapter 5 will discuss the growth of modified superlattices with digital alloy insertion and summarizes several directions for future plans.

Chapter 2

Metal-Organic Chemical Vapor Deposition

2.1 Epitaxy

Epitaxy, described by Royer in 1928 as "epitaxy occurs only when it involves the parallelism of two lattice planes that have networks of identical or quasi-identical form and of closely similar spacings", is a delicately controlled phase transition that produces a single crystalline solid [17]. Epitaxially grown deposits are formed through the nucleation of constituents and their properties will depend on the relation between these two phases: epitaxial layer (called epilayer) and substrate. There exist two kinds of epitaxy: homo-epitaxy and hetero-epitaxy. For both types, during the growth process, there is a chemically and structurally inhomogeneous interfacial region in which the diffusion, pyrolysis, adsorption, desorption, incorporation, and growth occur, playing a critical role on the material quality. Prior to an in-depth discussion about MOCVD, a brief description of the epitaxial growth process and the growth modes will be introduced, and the basic principles of MOCVD and the effect of various growth parameters will be discussed.

2.1.1 Crystallization Process

There are several epitaxial methods which can be classified by the type of utilized metastable phase: gas (MOCVD), liquid (liquid phase epitaxy, LPE), or solid (molecular beam epitaxy, MBE). Between this metastable phase and the substrate, there is a phase transition controlled by mass transport of constituents from the bulk

metastable phase toward the surface of the substrate. The driving forces to activate

the epitaxy process are determined by thermodynamics. Once the reaction starts,

thermal equilibrium will be violated and then epitaxy will occur. Fig. 2-1 depicts the

configuration of epitaxial growth system at different stages. In Fig. 2-1(a), prior to the

beginning of the growth, the metastable phase A consists of different precursors (for

MOCVD, they are metal-organic sources and hydrides for group III and V elements,

$t=t_0$

Phase A — Vapor metastable phase

— Interface

Phase B
(Substrate) — Solid stable phase

(a)

$t=t_1>t_0$

Phase A

Diffusion

Nucleation — Interfacial Region

Phase B
(Substrate) — Solid stable phase

(b)
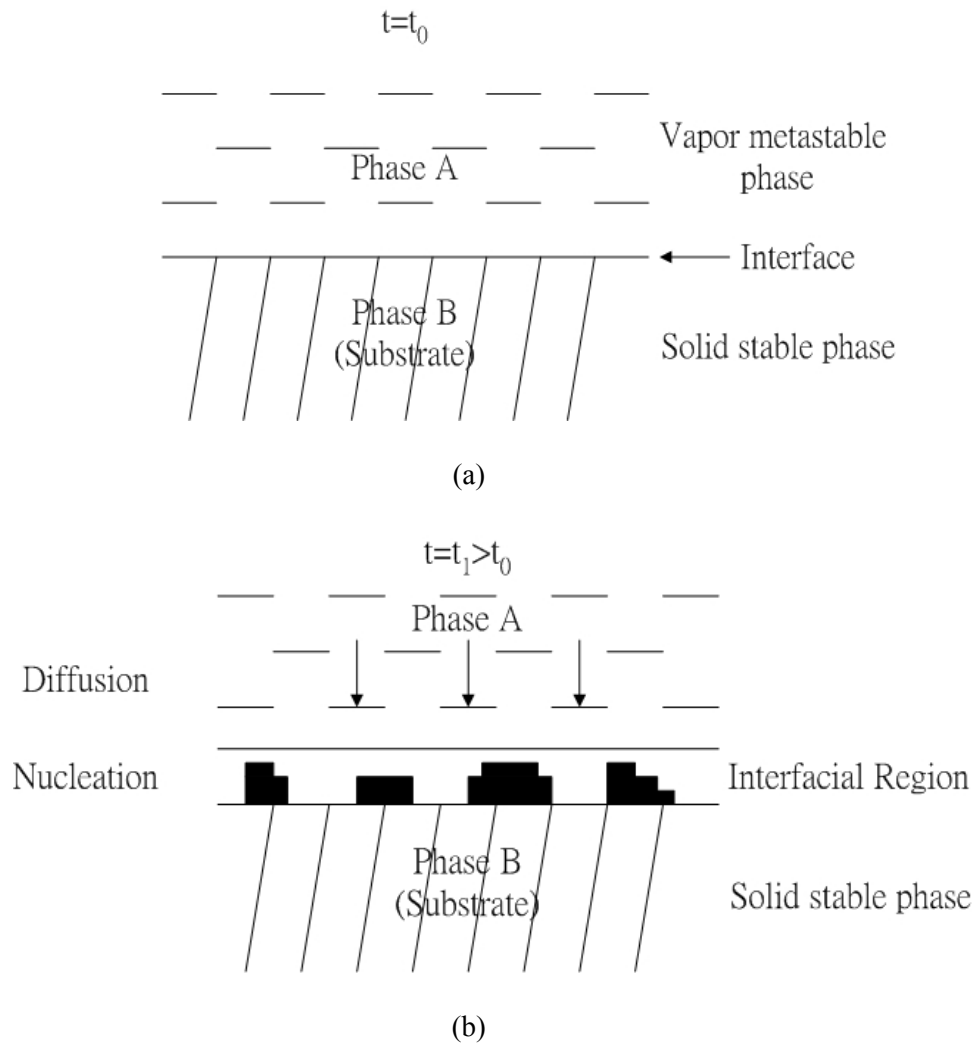
Fig. 2-1:   Schematic illustration of the epitaxial growth sequences at different time

periods of crystallization: (a) before growth started; (b) the nucleation period during which

the first monolayer is deposited.

$t=t_2>t_1$

Phase A

Diffusion →

Nucleation/Surface
Migration
Ordering/Desorption →

Interfacial Region

Phase B (Epilayer)   Grown Region

Solid stable phase

Phase B
(Substrate)

(c)

$t=t_3>t_2$

Phase A

Diffusion →

Nucleation/Surface
Migration
Ordering/Desorption →

Homogeneous Interface

Phase B (Epilayer)   Grown Region

Solid stable phase

Phase B
(Substrate)
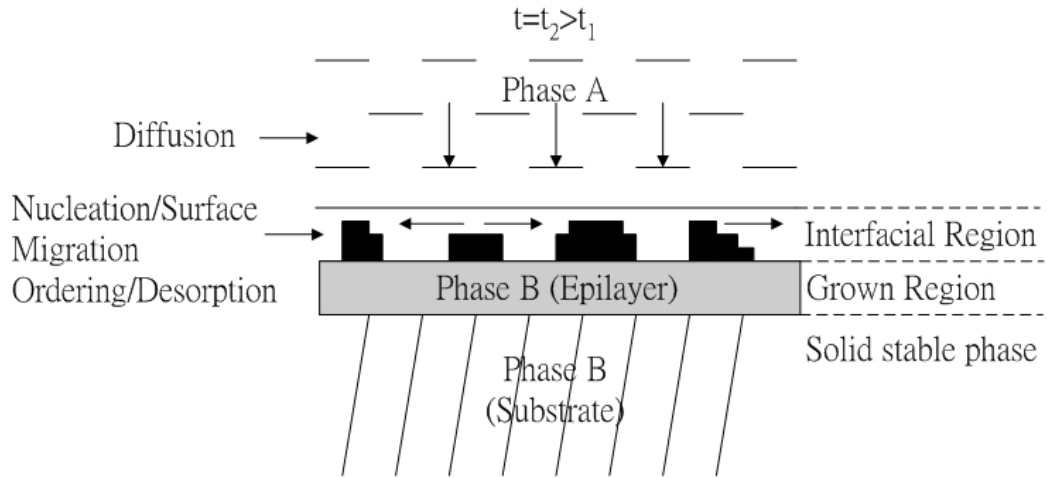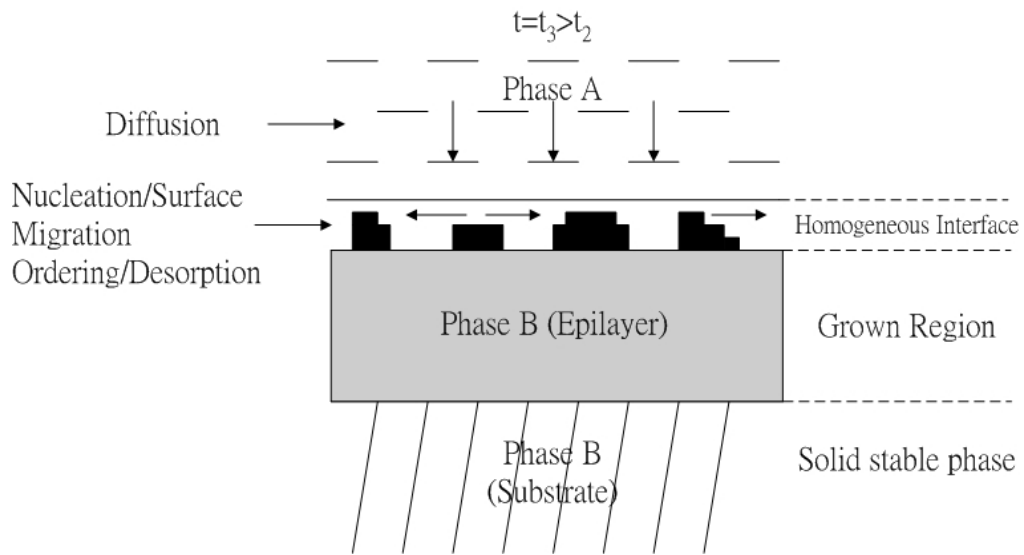
(d)

Fig. 2-1 (cont.):   (c) at an early stage of epitaxy a thin monolayer has been grown at the heterogeneous interface; (d) a fairly thick epilayer has been grown and the hetero-interface has lost its impact on the epitaxial process.

respectively) which will diffuse toward the surface of phase B. At this stage, though homogeneous reactions between precursors occur, they do not dominantly contribute to the growth. After time t_1, the precursors diffuse into the interfacial region to react

with each other at the specific temperature at which mass-transport-limited mechanism is the rate-limited step. The precursors pyrolyze at high temperature (> 500°C) and these decomposed constituents will combine via heterogeneous reactions to form the desired epitaxial layers near the surface of substrate (Fig. 2-1(b)). At this moment, the epitaxial process is initiated by nucleation and this heteroepitaxial interface is important for the whole epitaxial process.

After nucleation is activated, epitaxy will involve diffusion, desorption, ordering, and surface migration (Fig. 2-1 (c)). The last one is especially important for growing device-grade materials. While the growth type changes from homoepitaxial to heteroepitaxial mode at this stage, the initial heteroepitaxial interface has lost its impact on the growth process. The subsequent growth will follow the homoepitaxial mode until finished (Fig. 2-1 (d)). Here are some key processes in epitaxial growth: mass-transport, surface migration, incorporation and desorption. Their impacts will be discussed in the rest of this chapter and the next chapter.

2.1.2 Five Growth Modes

Except for the initial interface region between the substrate and epilayer, the whole growth process is essentially the same as that of the bulk materials. However, the different lattice constants, chemical interactions between these two regions such as segregation and inter-diffusion, and misfit defects result in different possible growth modes [18]. They are: Volmer-Weber (VW) mode, Frank-van der Merwe (FM) mode, Stranski-Krastanov (SK) mode, the columnar growth (CG) mode, and the step flow (SF) mode. These modes with which the epitaxy occurs are determined by

the level of lattice mismatch and interaction between the substrate and the epilayer, growth temperature, overpressure of the diffusing flux, and the adhesion and interface energy.
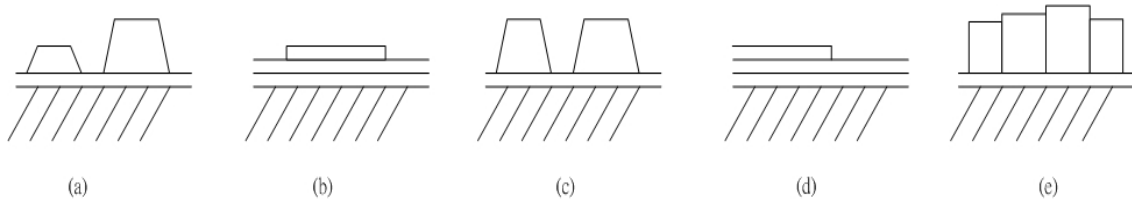
Fig. 2-2:   Illustration of five crystal growth modes: (a) VM; (b) FM; (c) SK; (d) SF; (e) CG mode.

These five growth modes are illustrated in Fig. 2-2. First, in the VW mode, the deposited molecules nucleate to form small clusters because of their stronger bonding forces with each other than with substrate atoms (Fig. 2-2(a)). Typically, this occurs when metals and insulators are grown. In contrast, the FM mode shows the opposite characteristics, in which the epitaxial atoms are more strongly bound to the substrate than to each other (Fig. 2-2(b)). It means that as the first diffusing atoms arrive near the surface, they prefer to stick to the atoms of the substrate to form a monolayer. The following incoming atoms will sit on this monolayer with somewhat smaller binding energy. This mode has been observed in gases, metals, metal-metal systems and semiconductor epitaxy. The SK mode is an intermediate case between the VW and FM modes and is generally observed in InAs/GaAs systems for the formation of quantum dots (Fig. 2-2(c)). The reason for forming the islands (or clusters) is that the interface energy and strain energy are both high. While the high interface energy will allow the initial layer-by-layer growth, the high strain energy will oppositely cause

the formation of dot arrays due to the relaxation via forming islands. For conventional semiconductor epitaxy, this mode is undesirable due to the effects of non-uniformity, composition variation, and worse interface quality.
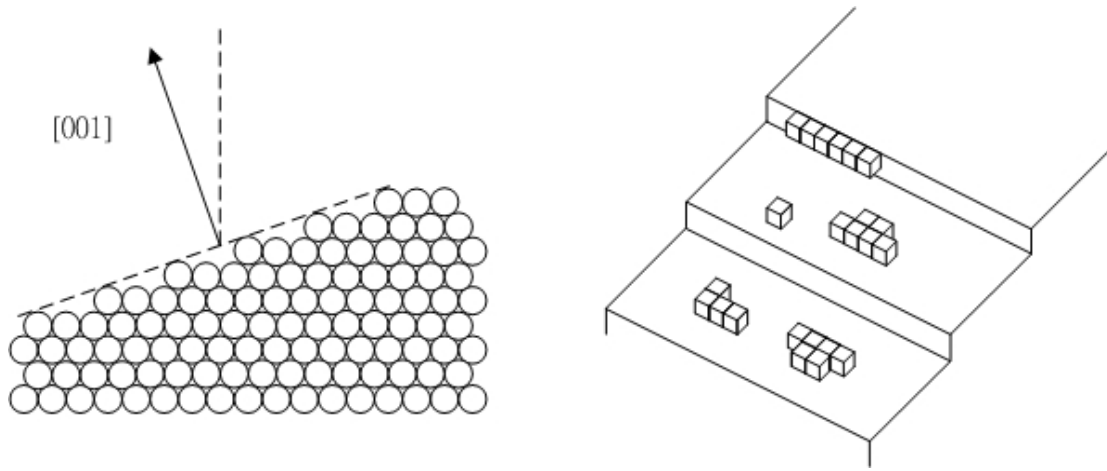
Fig. 2-3 : Left: misoriented crystal; Right: layer-by-layer growth process.

The fourth mode is SF mode, which is important for obtaining device-grade materials (Fig. 2-2(d)). Since the substrates usually do not have perfect crystalline structures, in which a misoriented angle can occur relative to the substrate surfaces, the growth mechanism will be different from the typical FM mode. In Fig. 2-3, we can see that near the surface of the misoriented substrate, atoms are not arranged in parallel with the interface; however, terraces and steps form. Therefore, two-dimensional nucleation may start on the vicinal planes with two possible growth modes. First, as the substrate temperature (growth temperature) increases or the influx of the constituent elements of the epilayer decreases, the atoms/molecules will have large mobility to migrate along the surface and be incorporated directly into the step edges, which in turn will improve the crystalline quality of the epilayer. However,

when the temperature decreases or the flux increases, the fast surface migration of the constituent elements will be prohibited, and islands and clusters may be formed to degrade the quality of the epilayer.

The last mode is CG mode, which is similar to VW and SK modes but fundamentally different (Fig. 2-2(e)). In VW or SK mode, as the epitaxy proceeds, the condensed islands tend to merge and then cover the whole substrate. Despite the appearance of structural defects or variation of the thickness across the surface, the islands or clusters will be continuously grown, merged, and distributed. But for the CG mode, the columns are formed without merger with other columns and are separated throughout the whole epitaxial process and easily fractured. For example, GaN exhibits this columnar structure in the form of whisker-like nanocrystals on Si substrate. The CG mode occurs due to low surface mobility for movement to the desired sites, leading to these highly defective columns of the grown epilayer and limiting the device application and its performance.

2.2   Metal-Organic Chemical Vapor Deposition (MOCVD)

In the early 1980s, people still argued whether MOCVD could compete with molecular beam epitaxy (MBE) with respect of the quality of grown epilayers such as thickness control, composition and composition uniformity, and the interface abruptness of the grown materials. However, MOCVD has been renowned for its high production capability and its larger variety of source materials (by using metalorganic compounds) compared to MBE, which is problematic for growing Nitride- and Phosphide-based III-V semiconductors (i.e. GaN, InP or InGaAsP), thus attracting

attention of researchers to develop atomic-scale MOCVD. The first successful quantum cascade lasers were made using MOCVD at the University of Sheffield in 2004 [9], which demonstrated the capability of MOCVD. Later the industry also successfully grew and fabricated room-temperature QCLs with high performance [10][11]. These results have encouraged our group and inspired us to study the properties of complicated quantum structures (~ 700 layer with near-atomic-scale). In this section, I will discuss the principles of MOCVD operation first. Although some physics or surface reactions are still unknown, the basic concepts, the source materials, and the major parameters for growth will be discussed in this section.

2.2.1 Principles of MOCVD Growth

MOCVD utilizes gas mixtures containing the constituent molecules which are also called precursors to grow the epilayers. Nowadays the carrier gas is hydrogen due to its purity. The growth temperature is $550^{\circ}\text{C} \sim 700^{\circ}\text{C}$ due to the stable growth rates provided in this regime. Low pressure (50 ~ 150 torr) operation is preferable for growing high-quality epitaxial layers, which will be discussed in the following subsection. Within this temperature range, the driving force is by thermodynamic and the reaction rates of surface kinetics are so high that diffusion is the rate-limiting step for the epitaxial process. In this regime, we can easily control the growth rate by adjusting the flow rate (partial pressure) of precursors with small variations of temperature and total reactor pressure.

Fig. 2-4 shows the sequential steps of a typical CVD process. There are four regions: substrate, interface/growth, transport, and carrier/sources regions. As seen in

16
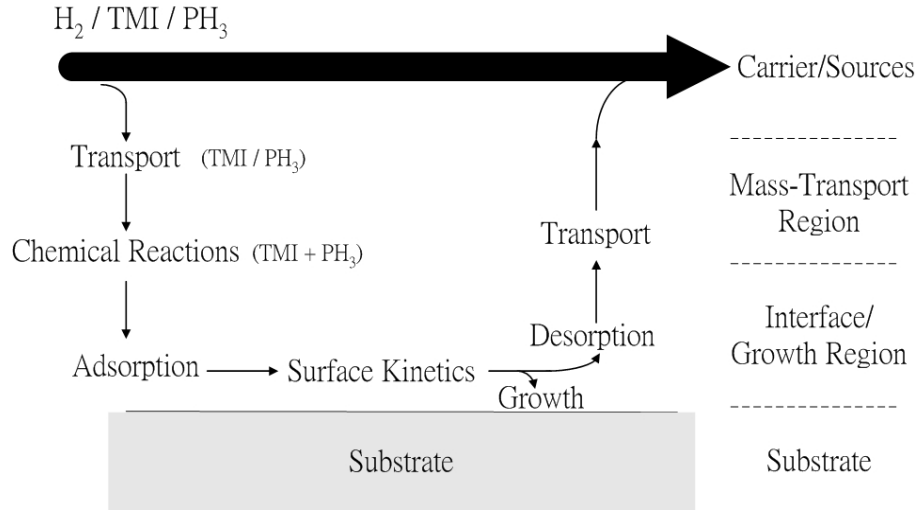
Fig. 2-4:   Schematic diagram of sequential steps of MOCVD growth.

this figure, the mixing gases containing all the required source elements (for example: $In(CH_3)_3$ and PH_3 for InP epitaxy) flow from the left side. Because of the concentration gradient of these two molecules between the source and the interface regions, $In(CH_3)_3$ and PH_3 will diffuse toward the surface of the substrate. Since the diffusion constants are weakly temperature-dependent, the growth rate is also expected to be weakly temperature-dependent. The diffused precursors will react with each other to form the desired compounds (i.e. InP) by the following chemical reaction:

$$In(CH_3)_3 + PH_3 \rightarrow InP + \text{organic by-products} \qquad (2.1)$$
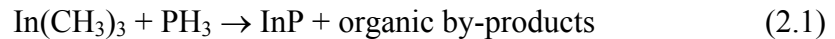
then followed by adsorption to the surface of the substrate. However, these resulting molecules are not fixed at their proper sites, instead they are mobile. The characteristics of the surface kinetics are not yet completely clear due to the lack of

17

in-situ measurement tools, but for some Al-based semiconductor materials like AlAs and InAlAs, kinetics indeed plays a critical role [19].

Although the deposited molecules are continuously supplied from the input sources, at high growth temperatures, desorption from the grown surfaces will definitely occur. Therefore, for compound epitaxial semiconductors growth by MOCVD, an overpressure of phosphorous or arsenic precursors must be applied to prevent the decomposition of P/As atoms when P or As is used as the group V constituent. The organic by-products such $In(CH_3)_2$, $InCH_3$, $(CH_3)_2$ and CH_3 etc., are transported from the interface region to the carrier gas out of the reactor to the waste system.

The above discussion is a very simple scenario for the MOCVD processes of thermodynamics, kinetics, and mass transport. The rate-limiting mechanism can be illustrated in Fig. 2-5, where the change of chemical potential from the source region to the substrate region is shown. The chemical potential is the driving force for the whole epitaxial process, thus determining the maximum growth rate. However, typical conditions for growth are far from this limit and, therefore the kinetics and mass-transport have more impact than thermodynamics does. In general, the chemical potential difference has been distributed during these four regions: sources transport, interface, and substrate region. Two extreme cases exist: one is interface-reaction limited and the other is mass-transport limited. The former shows the reaction rate near the surface is much slower than the mass-transport rate, in which the chemical potential drop mainly occurs at this region. This happens at low temperatures because the surface kinetic reaction rates are low compared to the diffusion rate. The

18

exponential behavior of the growth rate on temperature is unfavorable for stable growth. At present, most MOCVD machines have been operated at 550 ~ 700°C, during which the growth rate is almost constant. Within this range, the chemical reaction rates in the interface region are close to their maximal values and the mass-transport mechanism becomes the limiting factor. In this regime, once the molecules (precursors) arrive at the interface region, they react with each other immediately to form the epilayer. By adjusting the flow rate (partial pressure) of each precursor, the composition of ternary or quaternary compound epilayers can be controlled precisely by excluding the exponential dependence of temperature.
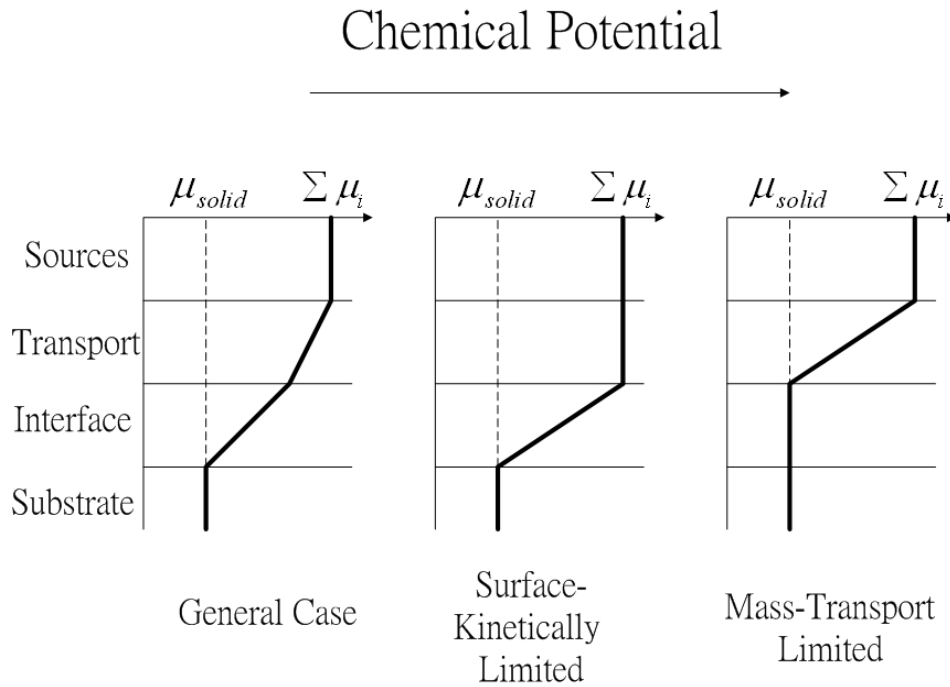
Fig. 2-5:   Plots of chemical potentials within four regions for different cases: general case, surface-kinetically limited, and mass-transport-limited.

2.2.2 System Configuration

Fig. 2-6 depicts a MOCVD apparatus, in which the most important pipes and sources, called bubblers, are shown. All gases including hydrides (group V), metalorganic sources (group III), and carrier gases (hydrogen in our system) are fed into the reactor. Usually the pipelines into the reactor are called "RUN" lines and there is another set called "VENT" lines into which the precursors are injected while they are not in use. The fast switches are required to obtain the good interface quality when quantum well structures are grown. A differential pressure line is necessarily installed for compensating the small pressure difference between RUN and VENT lines when switching occurs, preventing pressure fluctuations from different amount of precursors. Modern MOCVD machines use to control the fast switches and pressure/mass flow controllers, which in turn promotes the capability of MOCVD to grow atomic scales epilayers with similar reproducibility as in MBE.
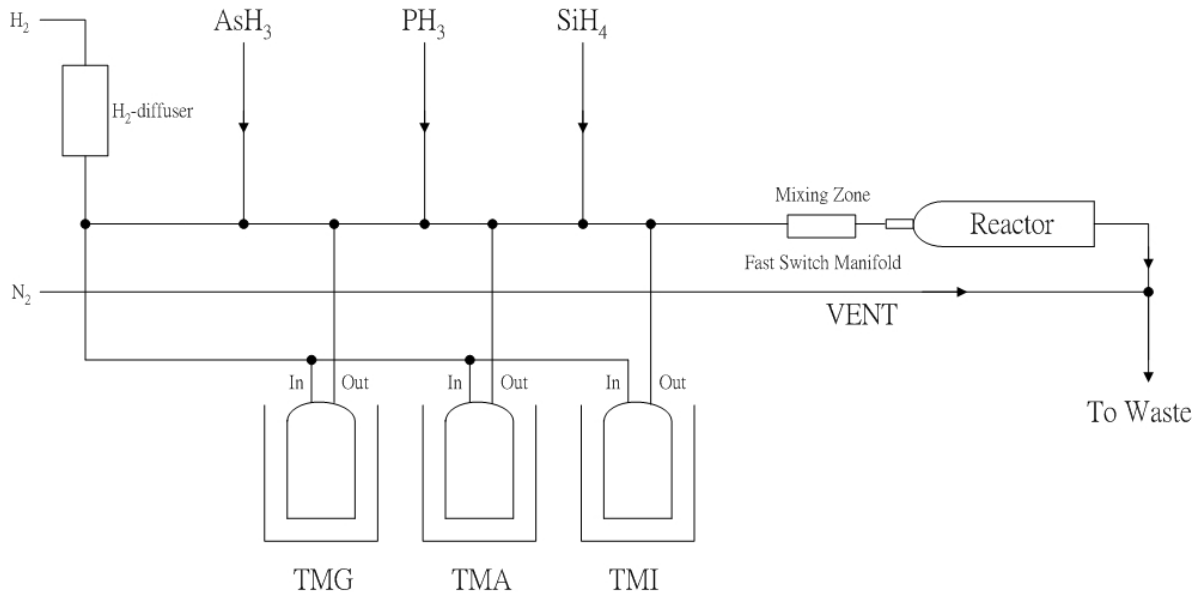
Fig. 2-6: Outline of a MOCVD apparatus.

Fig. 2-7 shows the schematics of a general horizontal reactor for MOCVD, in which the source molecules and carrier gas are coming from the gas inlet. Inside the reactor, there is a susceptor on which the samples are located. Heating is either done by a RF coil around the reactor or an infrared lamp from the bottom. In our MOCVD machine, three sets of IR lamps are employed to provide a uniform thermal gradient along the direction of the gas flow. This thermal gradient is important in that it will affect the gas flow distribution. From Fig. 2-7, there exists a tapered region between the gas inlet and the susceptor. This tapered design is critical for preventing turbulence before the gas flow arrives above the substrate, creating a uniform boundary layer with constant thickness. This boundary layer, between the substrate and the laminar flow layer, will affect the reaction rate, diffusion rate, composition, and uniformity. Usually the susceptor is designed to rotate for uniform epitaxial growth and the epilayer will then have uniform composition across the wafer.
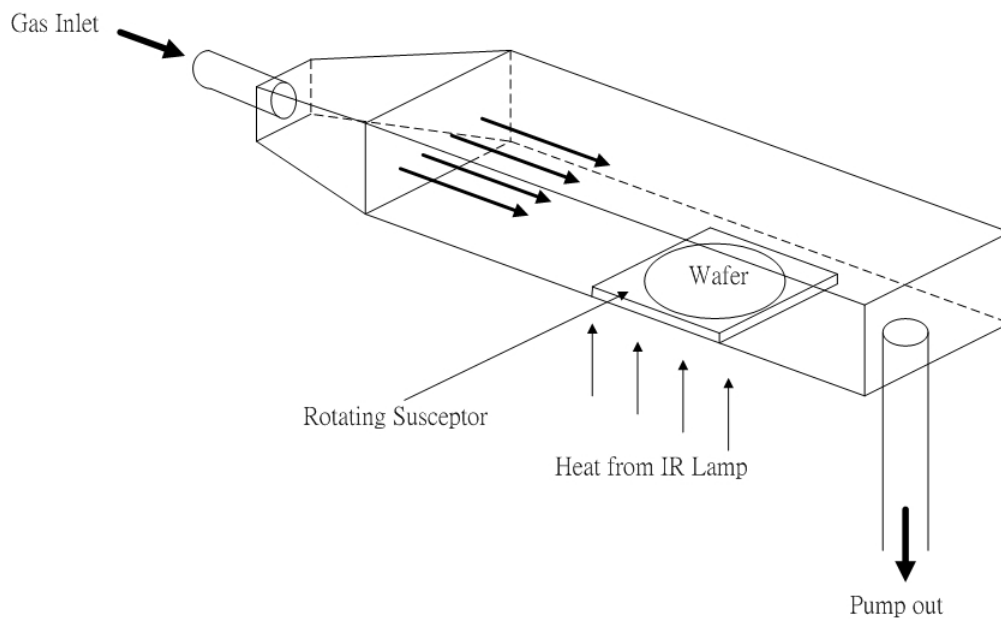
Fig. 2-7: Simple horizontal reactor configuration.

2.2.3 Source Materials

A variety of available source materials are one of the advantages of MOCVD over MBE. For example, growing phosphorous-containing materials such as InP and InGaAsP, are problematic for MBE because phosphorous is found to bounce around in the system, ultimately accumulating in the ultra vacuum pumps. That is the reason why buried heterostructures (BH) lasers are usually fabricated by MOCVD. Furthermore, for quantum cascade lasers, MOCVD is necessary for the thick cladding layers ($\sim 4\,\mu$m) due to its much higher growth rate. In principle, the metalorganic precursors are commonly designated by the MOCVD community by using M, E, P, and B to denote the radicals: methyl, ethyl, propyl, and butyl, respectively. Each metal atom of group-III precursors is bonded with three radicals forming a sp^2 hybridized structure. The most often used sources for group-III methyl-based compounds such as In(CH$_3$)$_3$, Ga(CH$_3$)$_3$, and Al(CH$_3$)$_3$, are abbreviated as TMI, TMG and TMA, respectively. Among their properties, the vapor pressure, the pyrolysis temperature, toxicity, and phase (solid or liquid) are critical for epitaxy. Methyl-based materials have advantages over other metalorganic sources such as their higher vapor pressure, purity, and reduced pre-reaction with hydrides. Higher vapor pressure can increase the growth rate, which in turn makes MOCVD more efficient and economic. In general, the lighter the molecules, the higher the vapor pressure. The vapor pressure can be expressed as

$$\log(p[\text{Torr}]) = a - \frac{b}{T} \tag{2.2}$$

where *a* and *b* are constants provided by vendors and *T* is the temperature of the precursor. The metalorganic sources can be stored in a so-called "bubbler" in terms of liquid or solid, through which their vapor molecules can be carried by hydrogen. By using a mass flow controller, we can adjust the amount of the carrier gas, which in turn, change the growth rate and composition. Alternatively, we can increase the bubbler temperatures for higher efficiency, but this will cause problems when the bath temperature becomes too high because vapor may condense in the colder tubing behind the bubbler. In such case, it becomes necessary to heat up the relevant pipes to stabilize the vapor pressure, and then the amount of the molecules injected into the reactor can be precisely controlled. The partial pressure in the reactor is given by

$$P_{MO} = \frac{F_{MO}}{F_{total}} \cdot \frac{P_{reactor}}{P_{bubbler}} \cdot P_{vapor}(T) \qquad (2.3)$$

where F_{MO} is the flow rate through the bubbler, F_{total} is the total flow rate in the reactor, $P_{reactor}$ is the operation pressure in the reactor, $P_{bubbler}$ is the pressure in the bubbler, $P_{vapor}(T)$ is the vapor pressure of metalorganic sources. Using (2.3), we have many options to adjust the growth rate and composition by changing F_{MO}, $P_{bubbler}$ and the bubbler temperature *T*.

For the group V sources, the pipe system is simpler because the most frequently used hydrides are pure phosphine (PH_3), arsine (AsH_3) and Nitride (NH_3), though sometimes hydrogen dilution lines are used. The partial pressure of the group V source materials is given by

$$P_{MO} = \frac{F_{hydride}}{F_{total}} \cdot P_{reactor} \qquad (2.4)$$

where $F_{hydride}$ is the flow rate of the hydride source.

The proper growth temperature is around 550°C to 700°C in that most precursor molecules start to decompose (pyrolyze) with almost constant rates. Generally, the metalorganic precursors have lower cracking temperature ($< 500^{\circ}$C) for 50% decomposition compared to hydrides ($PH_3 \sim 750^{\circ}$C, and $AsH_3 \sim 600^{\circ}$C), and within this temperature range, the variation of decomposition rate can be suppressed for stable growth. Decomposition can take place in the gas phase, which is called homogeneous reaction, or occur at the interface, what is called a heterogeneous reaction. Both reactions contribute to the growth but the latter is dominant because of two-dimensional geometry and the surface catalysis from the substrate. Although the details of the reaction are not understood, it is still necessary to know the possible reaction steps. The pyrolysis of TMG, for example, should be governed by the following reactions [17]:

$$Ga(CH_3)_3 \rightarrow Ga(CH_3)_2 + CH_3 \qquad (2.5)$$

$$Ga(CH_3)_2 \rightarrow GaCH_3 + CH_3 \qquad (2.6)$$

$$CH_3 + H_2 \rightarrow CH_4 + H \qquad (2.7)$$

$$GaCH_3 \rightarrow Ga + CH_3 \qquad (2.8)$$

$$Ga + H \rightarrow GaH \qquad (2.9)$$

$$GaH + H \rightarrow Ga + H_2 \qquad (2.10)$$

$$GaH + CH_3 \rightarrow Ga + CH_4 \tag{2.11}$$

$$GaCH_3 + CH_3 \rightarrow GaCH_2 + CH_4 \tag{2.12}$$
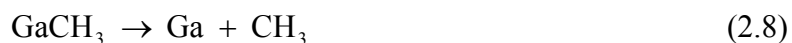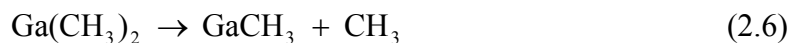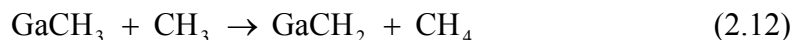
Despite detailed growth models with more 200 reactions required to be considered, certain reactions are believed to be the critical steps for the growth [17]. Unlike the metalorganic precursors, the possible reactions of the group V sources (hydride) are much simpler because only one decomposition mechanism is involved, generating three hydrogen atoms and an arsenic atom from one arsine molecule, and then reacting with the metalorganic molecule as

$$GaCH_3 + H + As \rightarrow GaAs + CH_4 \tag{2.11}$$
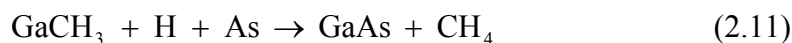
This simple mechanism explains why GaAs growth from TMG with hydride is successful but not with metalorganic group V source like TMAs because the direct As-H bond can make the GaAs growth occur more efficiently. A large concentration of methyl groups will remain on the surface with the following reaction

$$GaCH_3 + CH_3 \rightarrow GaCH_2 + CH_4 \tag{2.12}$$
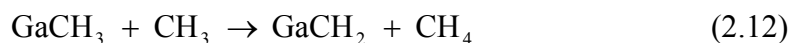
in which the carbons could be incorporated into the epilayer since CH_2 is not easily removed. This will happen if the temperature is low, because the decomposition efficiency at low temperature is not high enough to supply sufficient hydrogen atoms. That is the reason that if the impurity concentration is a concern for the device level,

good-quality materials can be grown at higher growth temperature with less impurity concentration. For InAlAs, high temperature growth is especially critical not only for the purity, but also for higher mobility of Al atoms to migrate across the surface to their crystalline sites. The latter will contribute to good morphology and improve the interfaces of the quantum well structures.

2.3   Effects of Macroscopic Parameters

Once the reactions between precursors are known, we will focus on the macroscopic parameters that allow us to control the growth conditions, such as growth temperature, pressure, V/III ratio, and growth rate. Typically, the growth temperature is the first one we need to decide before we start to grow. Because the pyrolysis of the precursors is strongly temperature-dependent and the surface kinetics is also temperature-related, despite a nearly constant growth rate, it is still necessary to determine the appropriate temperature for growing specific materials. If temperature is low, the pyrolysis process will be incomplete. The decomposition rate will have an exponential dependence on temperature, and thus the amount of the constituent molecules will also be temperature dependent, which will make control over alloy composition, epilayer uniformity, and growth rate more difficulty. On the other hand, ultra-high temperature will also reduce the growth rate. This can be explained by either the depletion of the reactants from the pre-reaction at the cold wall (the top side of the reactor) or desorption of the growing species from the substrate surface. In addition to the reduction of the growth rate, the high-temperature regime is very critical to the Al-containing alloys as mentioned before, for which the

reduction of oxygen is obtained due to the high volatility of Al suboxides, and carbon concentration can also be reduced. In contrast, if we want to have a p-type dopant, low temperature is desired for higher carbon doping [20].

Low reactor pressure operation (<200 torr) has been widely used because of its higher growth rate and better uniformity of epilayers, resulting from the larger mean free paths of constituent molecules. Larger mean free paths contribute to the growth of atomic-level quantum structures and much improved interface quality compared to operation at atmospheric pressure. Since all the growth in this work was under in the mid-temperature and low-pressure regime, the effect of growth rate and the V/III ratio become significant. In the past, the growth rate has been simply considered as a determining factor for total growth time; however, for growth of superlattices or quantum structures, the alternative thin layers require a lower growth rate. From the surface kinetics, if the growth rate increases, the deposited atoms have less time to move to their sites, which worsens the crystalline quality. Thus, a low growth rate can improve the quality of the epilayer and the interface abruptness. Typically, the growth rates are adjusted by the flow rates, input pressures, and the bubbler temperatures of the group III precursors. In this thesis, the impact of growth rate on optical properties of InGaAs epilayers will be discussed in Chapter 3, and the study of superlattices with different growth rates will also be included in Chapter 4.

Finally, the V/III ratio, despite not affecting the growth rate, has impact on the composition, crystal quality, surface morphology, and the optical properties of epitaxial materials. For example, in growing InAlAs or InGaAs epilayers, the V/III ratio needs to be larger than 20 in our MOCVD machine to prevent As atom

desorption from the surface. If the V/III ratio is too low, the surface will degrade and photoluminescence will be hardly measurable. Furthermore, because of the bonding characteristics between two group III atoms, the V/III ratio will affect the surface mobility and then the composition will change. For InAlAs growth, due to the large differences in bond strengths between Al-As and In-As, high mobility is required to obtain high-quality materials.

The consequence of variations in growth temperature, growth rate, and V/III ratio will be discussed in the Chapter 3 and by using X-ray, PL techniques and optical microscope, the structural, optical and surface morphology of InGaAs and InAlAs will be explored. Further discussion for obtaining high-quality superlattices will be given in Chapter 4.

Chapter 3

Growth and Characterization of InGaAs and InAlAs

In Chapter 2, the fundamentals and key factors of MOCVD have been introduced and discussed. Specific techniques are required to characterize crystal quality and to obtain the structural information such as the lattice mismatch condition. Typically, for binary semiconductors (e.g. InP or GaAs), thanks to the lattice match condition between the epilayer and the substrate being satisfied automatically, only the growth rate, impurity concentration, carrier mobility, and absorption need to be addressed when the epitaxy proceeds. However, for ternary or quaternary materials, each epilayer must have proper alloy composition to match the lattice constant of the substrate in order to prevent the relaxation of the grown layers. This is especially true for device applications, because if the strains between the epilayer and substrate are intolerable, the resulting misfit defects will degrade the device performance. For example, for the superlattice structures in quantum cascade lasers (QCLs) or quantum well infrared photodetectors (QWIPs) [21], the composition is of crucial importance not only due to the need for precise control over intersubband levels, but also due to many non-radiative impurities generated under highly strained condition. For QCLs, due to the characteristics of intersubband transitions, population inversion is achieved with more stringent restrictions on alloy composition compared to conventional interband semiconductor lasers. There are many ways to characterize the alloy composition and among them double-crystal X-ray diffraction (DCD) is the most powerful and quickest method [22]. In this chapter, the principle of X-ray diffraction

technique will be introduced first with its capability of probing the lattice mismatch condition that provides the information about the alloy composition, and of characterizing the quality of the epilayers from their intensity and linewidth. Moreover, X-ray diffraction is also a powerful tool to estimate the periodicity of superlattices from the satellite peaks accompanying their periodic structures. As a result, the growth condition of ternary InGaAs and InAlAs can be calibrated and adjusted in a short period. I will discuss the growth of InGaAs and InAlAs by changing several growth parameters such as flow rates of group III constituents, V/III ratio, and the growth temperature in the following sections. And in Chapter 4 the process for the optimization of growth parameters of InGaAs/InAlAs superlattices will be addressed.

3.1 Characterization by Using X-ray Diffraction

Since first used in 1917 by Compton, the double crystal diffractometer (DCD) has become a powerful tool for single crystals, especially true for epitaxially grown semiconductors. The DCD (Fig. 3-1), consisting of two crystals for increasing resolution by eliminating the wavelength dispersion and finite divergence angle, will generate a so-called "rocking curve" from the Bragg condition. The strain components caused from the lattice mismatch are given by [23]

$$\varepsilon_{xx} = \varepsilon_{yy} = \frac{a_0^S - a_0^E}{a_0^E}; \ \varepsilon_{zz} = \frac{a_z^E - a_0^E}{a_0^E} \tag{3.1}$$

where a_0^S and a_0^E are the relaxed lattice constants of the substrate and epilayer, respectively, and a_z^E is the strained lattice constant perpendicular to the growth plane.
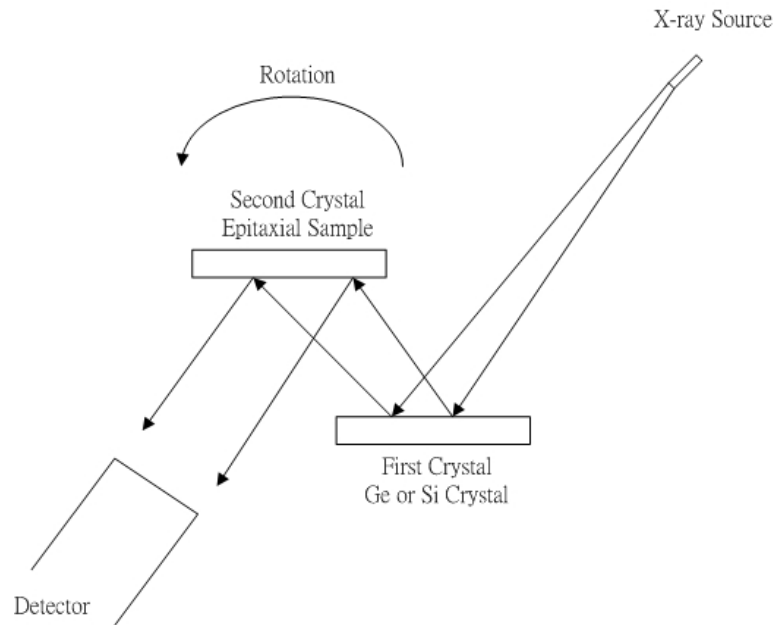
Fig. 3-1: Double Crystal X-ray configuration.
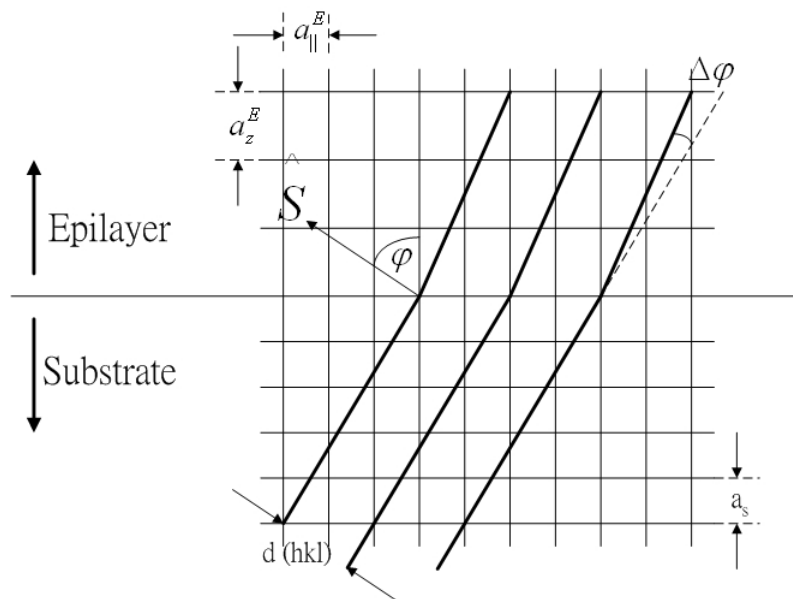
Fig. 3-2: Misorientation angle of crystal planes between the epilayer and substrate.

The X-ray strains are defined as

$$\left(\frac{\Delta a}{a}\right)_{\perp} = \frac{a_z^E - a_0^S}{a_0^S} = -\Delta\varphi\tan\varphi - \Delta\theta_B\cot\theta_B \qquad (3.2)$$

$$\left(\frac{\Delta a}{a}\right)_{\parallel} = \frac{a_{\parallel}^E - a_0^S}{a_0^S} = -\Delta\varphi\cot\varphi - \Delta\theta_B\cot\theta_B \qquad (3.3)$$

where $\Delta\theta$ is the angular separation between the Bragg peaks of epilayer and substrate, and θ_B the Bragg angle of the substrate, φ the angle between the lattice plane (hkl) and the substrate surface, and $\Delta\varphi$ the angular difference between the lattice plane orientation of the epilayer and substrate. Generally, the reflecting plane (hkl) may not be parallel to the surface (Fig. 3-2), and by employing (004) mode [22] based on the absence of difference of reflection angle and its strong reflection signal, the perpendicular strain can be reduced to $\left(\frac{\Delta a}{a}\right)_{\perp} = -\Delta\theta_B\cot\theta_B$. By measuring the difference of Bragg angles from X-ray rocking curves, the strain and a_z^E can be obtained. Then the composition of the ternary alloy (i.e. $In_xGa_{1-x}As$ and $In_yAl_{1-y}As$) can be derived by using Vegard's Law:

$$a_{InxGa(1-x)As} \equiv x \cdot a_{InAs} + (1-x) \cdot a_{GaAs} = a_0^E \qquad (3.4)$$

$$a_{InyAl(1-y)As} \equiv y \cdot a_{InAs} + (1-y) \cdot a_{AlAs} = a_0^E \qquad (3.5)$$

In addition to the alloy composition, X-ray diffraction can also characterize the quality of the epilayers from the FWHM of the Bragg reflection, which strongly depends on the thickness of the epilayer and their composition uniformity. There are two factors affecting the thickness dependence: absorption and interference. Typically, the absorption length is on the order $<100\mu$m and for interference, the effective penetrating length is on the order $<10\mu$m [23]. The reflected X-ray intensity is thus determined by both effects. However, if the thickness of the epilayer is below 1μm, the information extracted from the FWHM should be interpreted carefully with knowledge of film thickness. In our experiments, all comparisons have been made with the same thickness to eliminate this uncertainty.

From X-ray rocking curve, the lattice mismatch condition and the information about crystal quality are obtained without any sample preparation step such as cleaning or etching. Furthermore, the capability of X-ray diffraction for the characterization of the superlattice structures was also demonstrated [24]. The diffraction patterns of a periodic structure show a series of satellite peaks accompanying the main peak, which represents the net strain of the whole structure relative to the substrate. The Bragg condition can be modified as

$$\frac{2\sin\theta_m}{\lambda} = \frac{m}{a_0^E} + \frac{n}{D}$$

(3.6)

which m and n are integer indexes and the D is the superlattice period. By Taylor expansion, we obtain

$$D = \frac{\lambda}{2(\cos\theta)\Delta\theta} \qquad\qquad (3.7)$$

We can deduce the periodicity from the rocking curves of the superlattices, in which the intensity of the higher order peaks and the uniformity of the periodicity indicate the quality of the structures. Once the period number increases, the signal will be stronger. Fig. 3-3 illustrates the schematic diagram of the X-ray diffraction patterns of a superlattice with two constituent materials A and B, with lattice constant a_A and a_B,
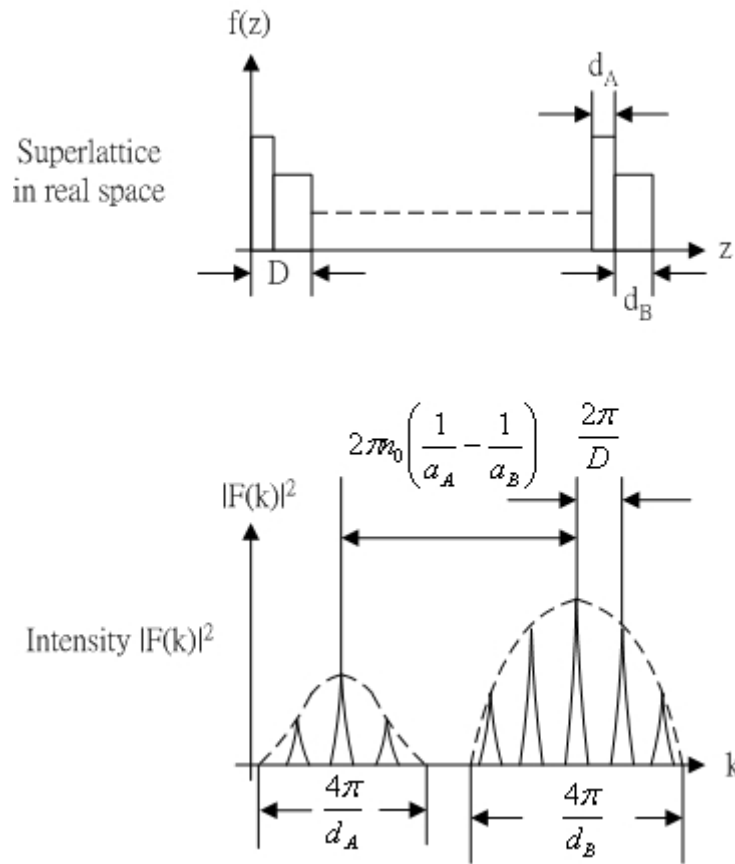
Fig. 3-3: The superlattice structure in real space and k space.

the layer thickness d_A and d_B, and the period $D = d_A + d_B$. For InGaAs/InAlAs superlattices, if the alloy compositions of these two materials are the same, the center

of the two envelops will be at the same position and the distance between the satellite peaks gives the information about the period D. As the number of period increases, the linewidth of each satellite peak decreases with increasing intensity. This capability is essential to quantum cascade lasers because of the stringent requirement for uniformity of the periodic structure that can significantly affect the population inversion between subbands. In Chapter 4, it will be made clear that X-ray and photoluminescence (PL) are two important and quick tools for characterizing the superlattice structures and quantum cascade lasers.

3.2   Lattice Mismatch vs. Flow Rates of Group-III Materials

By using double crystal X-ray diffraction, the lattice mismatch condition can be obtained for the difference of the Bragg peak positions between the epilayer and substrate. Due to the thickness-dependent property of X-ray signals, all the comparisons were completed with the same thickness.

To characterize the lattice mismatch condition (alloy composition), we keep all parameters constant except for the flow rates of TMG (or TMA) for InGaAs (InAlAs). The bubbler temperatures of TMI and TMG are 15°C and -8°C for the growth of InGaAs epilayers, the growth temperature 625°C, the reactor pressure 100 torr, AsH$_3$ flow rate 30 sccm, TMI flow rate 400 sccm, and the partial pressures of TMI and TMG pipelines are 1000 and 1500 torr. The growth rate was ~ 8.5 Å/s, the thickness of epilayer was ~ 4000 Å, and all epilayers were grown on (001) Fe-doped InP substrates. The TMG flow rate was changed from 3 to 10 sccm, and Fig. 3-4 shows the X-ray rocking curves of In$_x$Ga$_{1-x}$As with strain from -0.644% to 0.906%

corresponding to TMG flow rate from 3 to 10 sccm. In Fig. 3-4 (a), due to the large

strain from misfit defects existing at the interface between the epilayer and substrate,

the linewidth is broad (~ 286.4") and the intensity is weak. In Fig. 3-4 (c) and (d),

much narrower linewidth and stronger intensity were obtained because of its

extremely small strain.

(a)

(b)

(c)

(d)
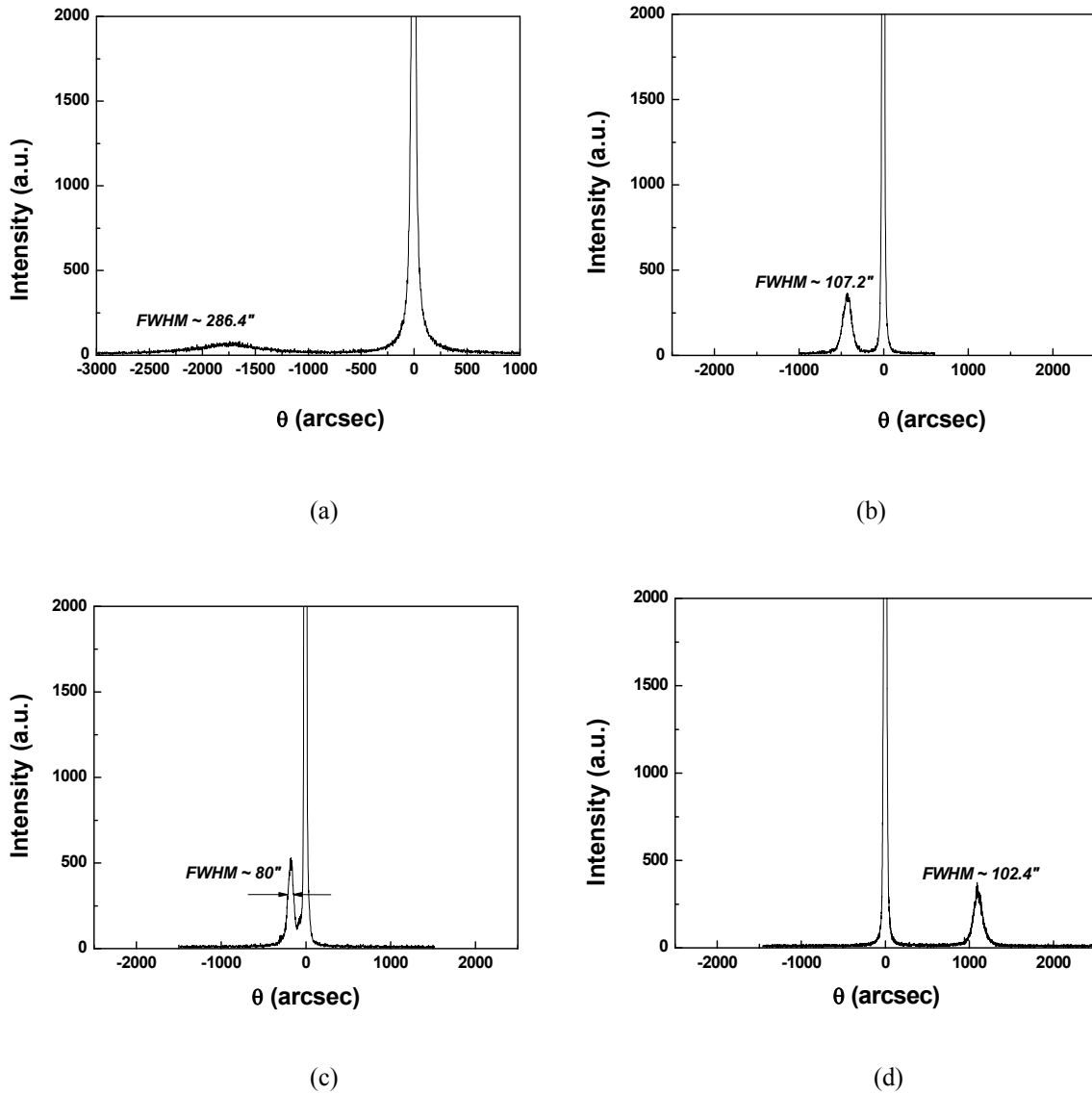
Fig. 3-4:   X-ray rocking curves of $In_xGa_{1-x}As$ with strain (a) -0.635 %, (b) -0.172 %; (c) -0.02 %; (d) 0.432 %.

Fig. 3-5 illustrates the lattice mismatch condition versus TMG flow rate. As expected, once the TMG flow increases, the alloy composition x decreases with lattice mismatch changing from negative to positive, which corresponds compressive strain (In-rich) to tensile strain (Ga-rich). When the magnitude of lattice mismatch smaller than 0.5%, the relation between the strain and the TMG flow is almost constant, allowing us to adjust the composition of Ga linearly.
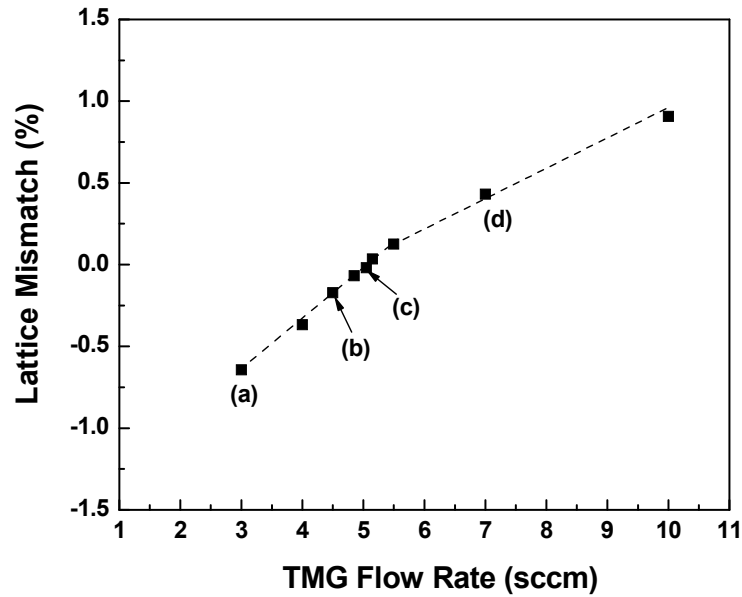
Fig. 3-5: The lattice mismatch of $In_xGa_{1-x}As$ epilayers versus TMG flow rate. The (a) ~ (d) correspond the points in Fig. 3-4 (a) ~ (d)

If TMG flow rate is too large, owing to the large tensile strain resulting from misfit defects, the composition control becomes more difficult. Moreover, the In incorporation coefficient defined as [25]

$$K = \frac{x}{p_{In}/(p_{In} + p_{Ga})} \tag{3.8}$$

also changes with TMG flow rate (Fig. 3-6). Because more Ga atoms exist on the surface with higher TMG flow rate, the migration of In atoms will be affected by these Ga atoms, suppressing the In incorporation ability. Besides, as the TMG flow rate increases, the corresponding decrease of V/III ratio could contribute a second-order effect on In incorporation coefficient, which will be discussed in the next section. Though very small variation in V/III ratio in this case (47 ~ 51), the V/III ratio indeed influences the In incorporation coefficient and in turn, composition control. In summary, the reduction of In incorporation along with the increasing TMG flow rate would be from the competition of In atoms with Ga atoms and the accordingly reduced V/III ratio. The calculated In incorporation coefficients are 0.65 ~ 0.8, smaller than unity, due to the smaller diffusion coefficient of TMI compared to TMG [25].
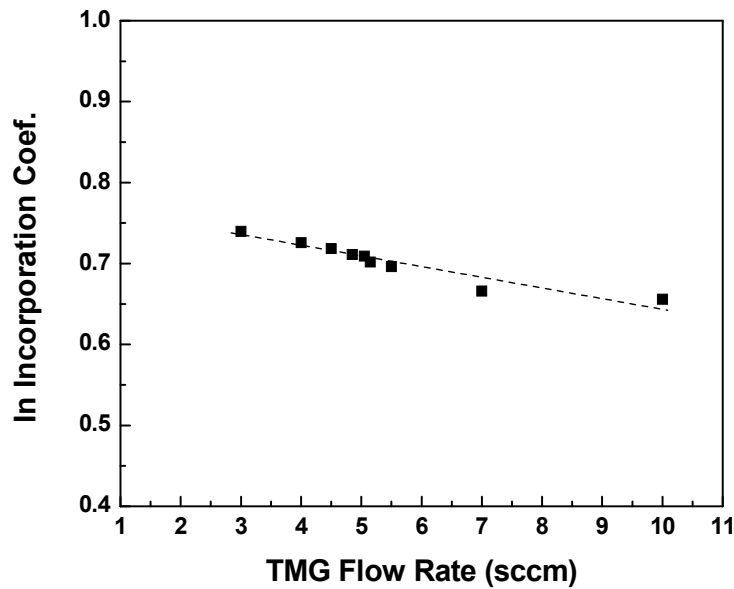
Fig. 3-6:   In incorporation coefficient of $In_xGa_{1-x}As$ epilayers versus TMG flow rate.
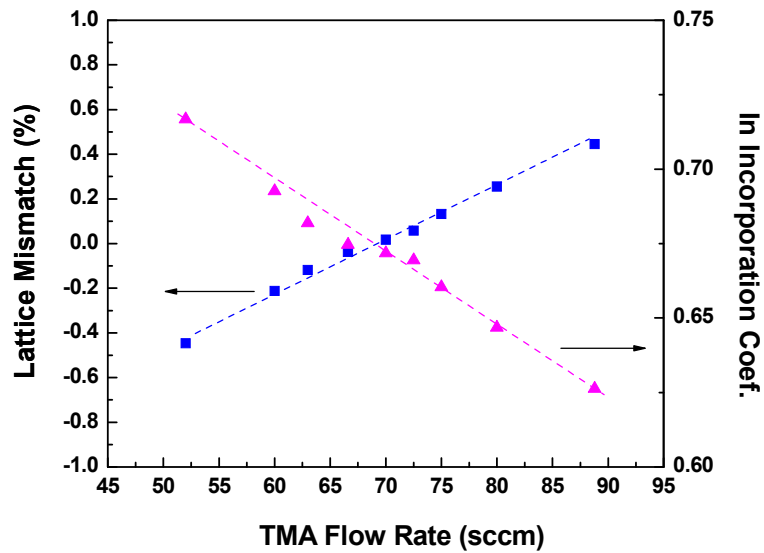
Fig. 3-7: The lattice mismatch and In incorporation of $In_yAl_{1-y}As$ epilayers versus TMA flow rate.

For InAlAs epitaxial growth, the growth parameters are as follows: TMA flow rate changed from 52 to 88.8 sccm, TMI flow rate 300 sccm, AsH_3 flow rate 50 sccm, bubble temperatures of TMA and TMI 10 and 25^oC, growth temperature 650^oC, and the growth rate ~ 6.2 Å/s. The reactor pressure and the partial pressures of TMI and TMG pipelines are kept the same as the case of InGaAs and in the subsequent discussions. Expectedly, similar behavior was shown in Fig. 3-7, in which the lattice mismatch and In incorporation coefficient versus TMA flow rates are shown. The In incorporation coefficients in InAlAs are all smaller than that of InGaAs (see Fig. 3-8) because of the larger difference of bonding strength between In-As and Al-As in InAlAs than that of In-As and Ga-As. In-As bonds are much weaker than the Al-As bonds and consequently, In atoms have a weaker tendency to be incorporated into the

39

epilayer. Thus, smaller incorporation coefficients were obtained in InAlAs compared to InGaAs.
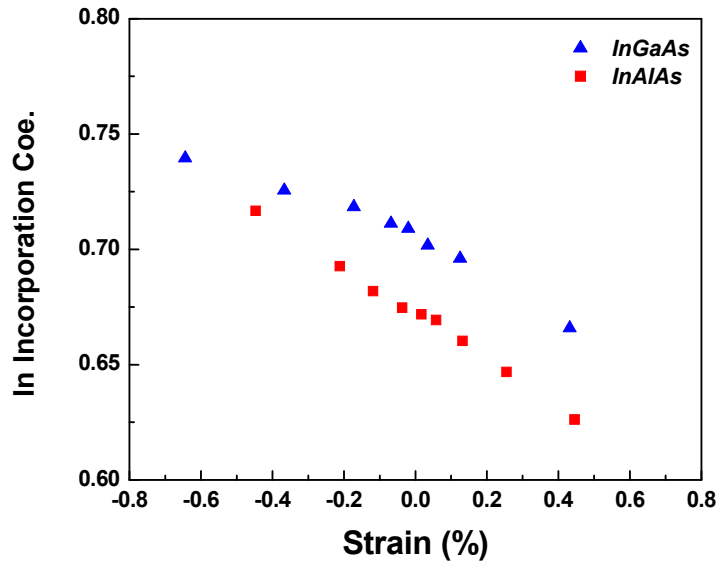
Fig. 3-8:   The In incorporation coefficients vs lattice mismatch of $In_xGa_{1-x}As$ and $In_yAl_{1-y}As$.

Not only is the lattice mismatch condition known, but information about crystal quality can also be extracted from X-ray rocking curves from their peak intensity and linewidth. Fig. 3-9 shows the linewidth and the relative peak intensity (which is defined as the peak intensity of epilayer divided by the substrate peak) versus lattice mismatch for InGaAs epilayers. The broadened linewidth and weaker intensity indicate the importance of the lattice mismatch on the crystal quality. If the strain is too large, the X-ray signal is weaker. For device applications, it is required to have precise control over alloy compositions. By careful calibration before devices are grown, almost perfectly lattice-matched alloys can be obtained repeatedly with

extremely small deviation. Superlattices or quantum cascade structures are typical grown with strains smaller than $|5 \times 10^{-4}|$ in this thesis.
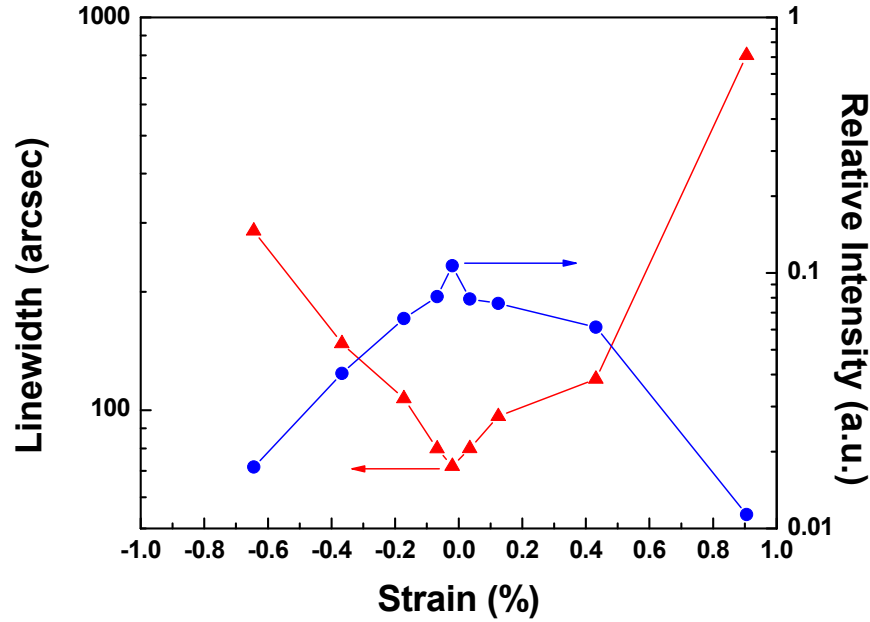
Fig. 3-9: The linewidth and relative intensity of X-ray rocking curves vs. lattice mismatch of $In_xGa_{1-x}As$.

3.3   Lattice Mismatch vs. V/III Ratio and Growth Temperature

In the previous section, the relation between the lattice mismatch and precursor flow rates was discussed. Although the lattice match condition can be obtained easily by adjusting TMG or TMA flow rate, other growth parameters can also influence the strains, such as V/III ratio and growth temperature. In this section, the effects of the V/III ratio and growth temperature will be discussed by using Double Crystal X-ray technique.

3.3.1 V/III Ratio

For the study of the influence of V/III ratio on lattice mismatch condition, the growth parameters are as follows: TMG flow rate 12.8 sccm, TMI flow rate 300 sccm, bubbler temperature of TMG and TMI 25 and -7.5°C, growth temperature 650°C, and the growth rate is 5.92 Å/s. In Fig. 3-10, when the V/III ratio increases, the alloy composition x of $In_xGa_{1-x}As$ decreases slightly. This effect can be understood from the surface kinetics aspect. Once the V/III ratio increases, the In atoms will tend to combine with As atoms on the surface more easily. This is due to the weaker bonding strength of In-As compared with Ga-As. If the AsH_3 pressure is increased, extra As atoms will become available for combining with In, resulting in a higher composition of InAs compounds. From Fig. 3-10, the In incorporation coefficients slightly change from lattice-matched to 1×10^{-3} with only 2% deviation by increasing V/III ratio from 43 to 130.
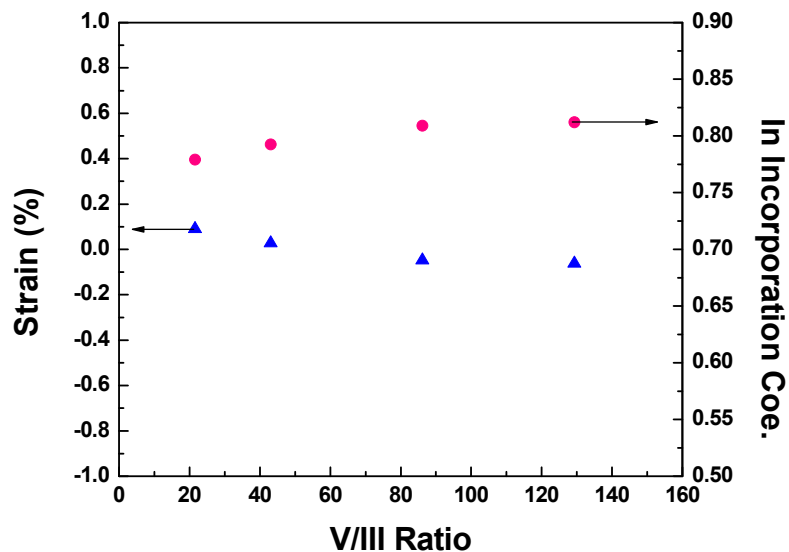
Fig. 3-10: The relation between strain and In incorporation coefficient vs. V/III ratio for InGaAs.

For InAlAs, the increase of In incorporation coefficient is more pronounced than that of InGaAs (Fig. 3-11). The strongly V/III ratio-dependent behavior of lattice mismatch can be explained as follows: at low V/III ratio, fewer As atoms appear near the grown surface. Because of the stronger bond strength of Al-As than In-As, more As atoms bond to Al statistically, resulting in more AlAs. Consequently, the In incorporation coefficient is reduced when V/III decreases [26]. In contrast, if the V/III ratio increases, though the tendency of As to combining with Al is still high, because of this oversupply, In atoms have more chance to bond with As atoms. Therefore, the In incorporation coefficient increases with V/III ratio.
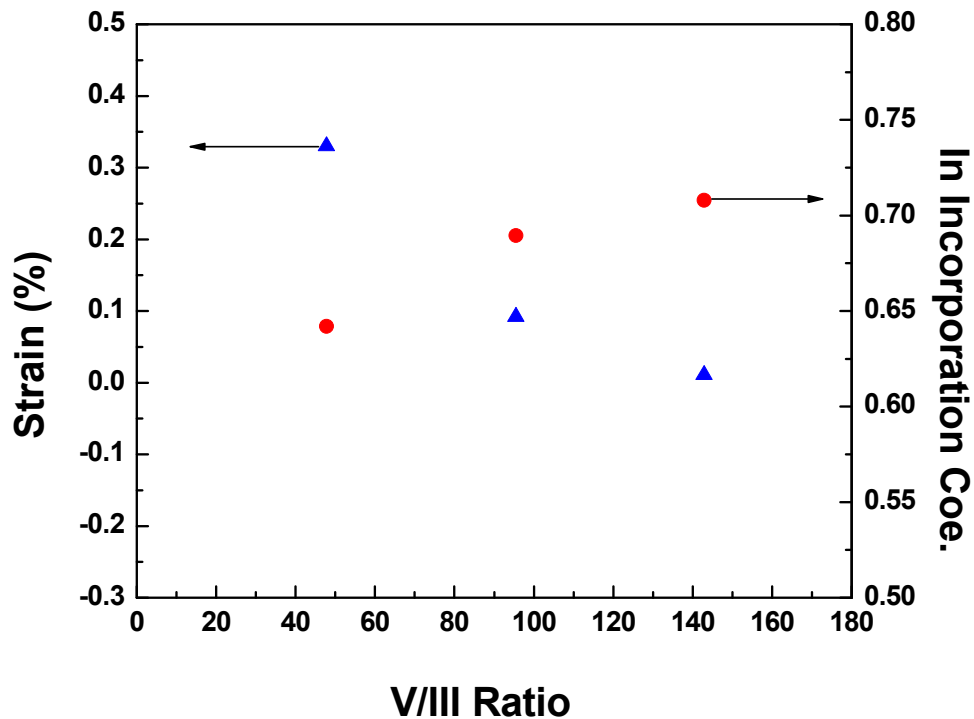
Fig. 3-11: The relation between strain and In incorporation coefficient vs. V/III ratio for InAlAs.

3.3.2 Growth Temperature

Generally, the growth temperature in MOCVD is at $550 \sim 700^{\circ}$C. While the decomposition rates of precursors are not constant and the growth mode will become surface-kinetics limited at low temperature, the high temperature regime also has the problem of surface degradation and a reduction of growth efficiency. However, for InP-matched materials such as InGaAs and InAlAs, the impurity concentration will decrease as the temperature increases [27]. Especially for InAlAs, high temperature is necessary due to the presence of oxygen and carbon with high concentrations in Al sources. Study of the effect of growth temperature on the lattice mismatch condition was conducted with all other growth parameters kept unchanged.
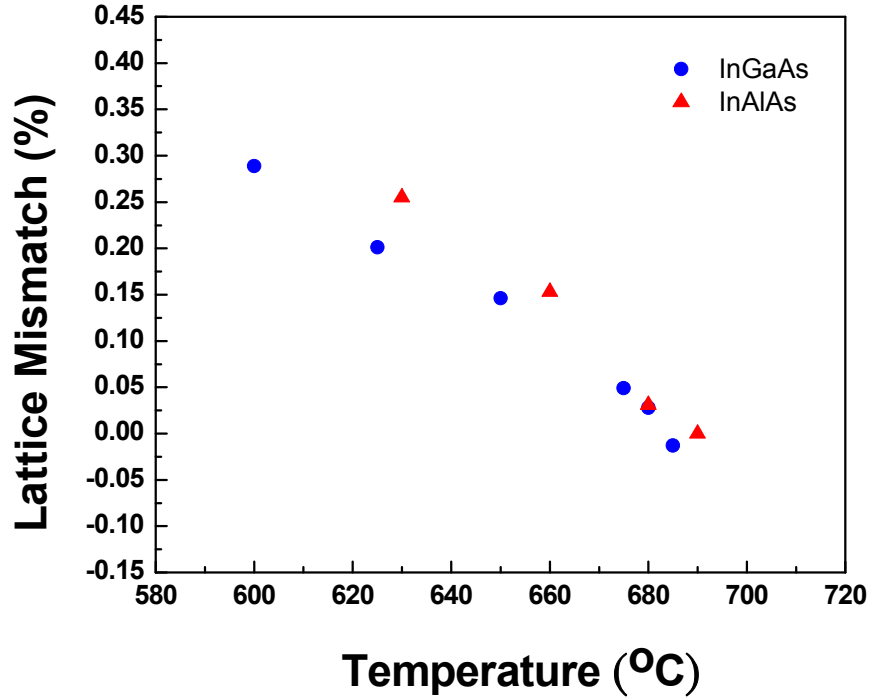
Fig. 3-12: The lattice mismatch vs. growth temperature for InGaAs and InAlAs.
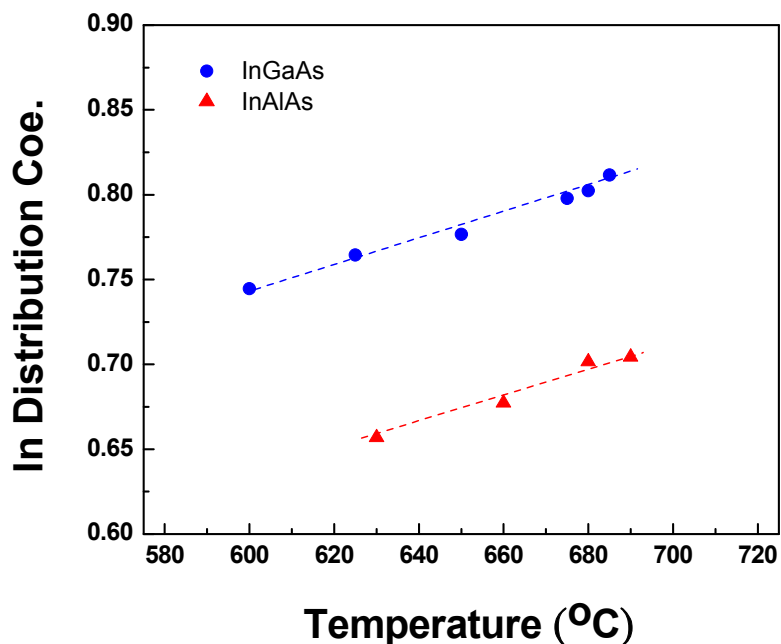
Fig. 3-13: In incorporation coefficient vs. growth temperature for InGaAs and InAlAs.

Similarly to the V/III ratio, growth temperature has a similar effect on lattice mismatch. As the temperature increases, the strain will become more compressive, and inversely, once the temperature decreases, the epilayer becomes more tensile. Fig. 3-12 shows the relation between the temperature and the lattice mismatch condition for InGaAs and InAlAs. This can be understood as follows [28]: at low temperature TMI and AsH_3 tend to react to form adducts whose diffusion flux to the growth surface is smaller because of their small diffusion coefficient, and this in turn reduces the amount of TMI arriving at the surface. At higher temperatures, the adducts become less stable and begin to decompose, increasing the In surface concentration. Fig. 3-13, shows the relation between In incorporation coefficient and the growth temperature. Some groups reported the opposite trend that increasing temperature

leads to a decrease in In incorporation [26]. This is due to the removal of In atoms in the gas phase by the increased pre-reaction, or due to the enhanced In desorption from the surface at higher temperature. However, the above discussion did not consider the influence of temperature on the V/III ratio which will be affected accordingly in that pyrolysis of AsH_3 is not complete below 700^oC. As the temperature increases, the decomposition of AsH_3 also increases [25], and those extra As atoms will enhance the In incorporation rate, which was discussed in the previous section. As a result, the In incorporation will be increased further by this second-order effect.

In summary, there are three mechanisms which can influence the In incorporation rate: (1) Adducts formed by TMI and AsH_3 reduce the amount of In atoms arriving at the surface, enhancing the In incorporation with increasing temperature because of the larger diffusion coefficient of the formed adducts and their higher cracking rate; (2) Pre-reaction between the TMI and AsH_3 and the In desorption will increases with temperature, resulting in In deficiency at higher temperature; (3) The dependence of AsH_3 cracking efficiency on temperature also plays a supporting role for (1), restricting the surface migration of Al (Ga) atoms and therefore, higher In incorporation. It appears that in our MOCVD system, the presence of adducts and the resulting increased As atoms with increasing temperature, have enormous impacts on In incorporation compared with the pre-reaction between TMI and AsH_3, and In desorption rate.

46

Chapter 4

Detailed Studies of InGaAs, InAlAs, and InGaAs/InAlAs Superlattices

In Chapter 3, the epitaxial growth of $In_xGa_{1-x}As$ and $In_yAl_{1-y}As$ and their characterization by X-ray were discussed. By controlling the growth parameters such as growth temperature, V/III ratio, the flow rates of group III precursors (TMG or TMA), bubbler temperatures and the partial pressures of group III precursors, we can obtain $In_xGa_{1-x}As$ and $In_yAl_{1-y}As$ (x ~ 0.53 and y ~ 0.52) lattice-matched to InP. Typically the bubbler temperatures have been set constant because the metal-organic sources take long time to stabilize, and we adjust their flow rates and partial pressures. The growth rate is determined by group III precursors. For example, when we grow $In_xGa_{1-x}As$, based on our experience, In bubbler temperature 25^oC, In-line partial pressure 1000 torr, the flow rate 300 sccm and reactor pressure 100 torr could give us a growth rate of 4 Å/s. Then based on the procedure in Chapter 3, we can easily change V/III ratio, growth temperature, and the flow rate of TMG to obtain the desired alloy composition. At this chapter, we focus on the crystal quality, optical property, and the surface morphology of InGaAs and InAlAs epilayers with strains kept smaller than $\pm 1 \times 10^{-3}$, which minimizes the effect caused by misfit defects. First, a study of the optical properties of InGaAs was conducted and the maximum growth temperature was successfully raised to 675^oC, which is high so that the impurities can be reduced dramatically [29]. In addition, the effects of V/III ratio and growth rate on

their PL intensity were also investigated. Then we focus on the structural properties and morphologies of InAlAs. From X-ray rocking curves and high-resolution microscopy, the optimized growth conditions for InAlAs have been found at mid-temperatures (630 ~ 675°C) with V/III ratio no larger than 150. Finally, many superlattices were grown to look for the optimized growth conditions for quantum cascade lasers. The results showed that even with very high growth rate, the PL intensity of the superlattices grown at high temperature is comparable to those grown at low growth rate. The impurity concentration and the growth time for quantum cascade lasers can be reduced at the same time without compromise of device performance.

4.1   Optimization of InGaAs Epilayers

4.1.1   Impacts of Temperature and V/III Ratio

The growth temperature has profound effects on the optical properties of InGaAs epilayers [25]. To stabilize the cracking efficiency of TMI, TMG and AsH$_3$, a growth temperature above 550°C is necessarily used. Furthermore, the high temperature is believed to be an effective way to reduce impurity concentration of epilayers [30]. However, at high temperatures, surface decomposition occurs and the PL intensity decreases dramatically, which can be understood by As atom desorption from the grown surface [31]. Therefore, there exists a window of growth temperatures not only to reduce impurities, but also to avoid surface decomposition. In this subsection, we focus on the effect of the growth temperature on the PL spectra of the epilayers. By using the room-temperature PL technique, it is convenient to get the

information about the quality of epilayers. Our target is to extend the maximum growth temperature to provide excellent epilayers without surface degradation of InGaAs materials.
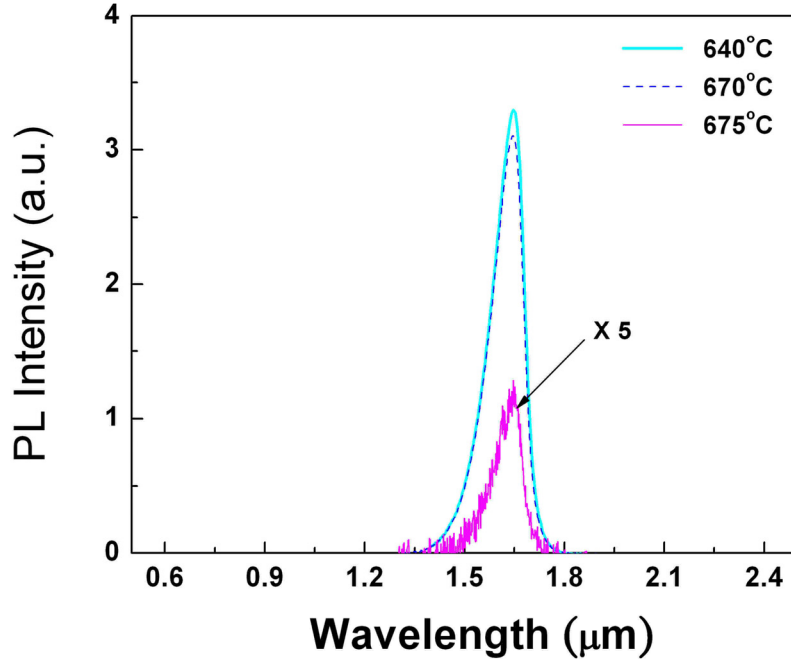
Fig. 4-1: PL Spectra of InGaAs epilayers grown at 640, 670, and 675°C with V/III~45.

First, we keep the growth parameters constant except for the growth temperature. The V/III ratio is ~ 45, the growth rate is 4 Å/s. The reactor pressure is 76 torr and the thickness of epilayers is ~ 3500 Å. All the samples were grown with the magnitude of their strains smaller 1×10^{-3} to prevent the effect from the misfit defects which occurs at large strains. Fig. 4-1 shows the PL spectra of InGaAs grown at 640, 670, and 675°C, in which the peak intensity decreases as the temperature is above 675°C, corresponding to the degradation of InGaAs epilayers at high growth

temperature. Optical images from a high-precision microscope provide further evidence for surface decomposition (Fig. 4-2). While the surface of epilayer grown at 640°C looks perfectly flat in Fig.4-2 (a), the surface image of (b) apparently shows much worse morphology when grown at high temperature (680°C).

(a)   (b)
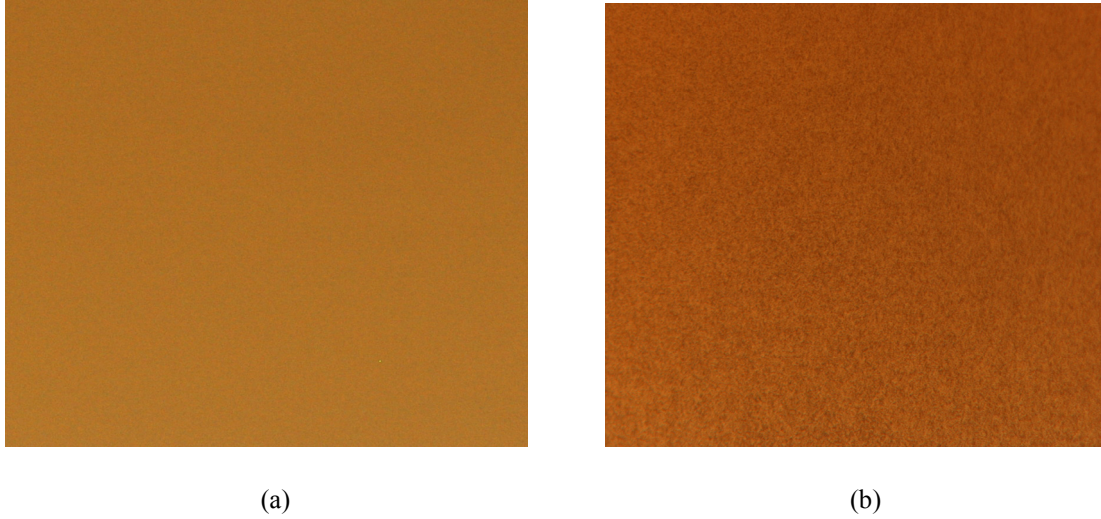
Fig. 4-2:   Optical images of InGaAs epilayers grown at (a) 640 and (b) 680°C.

To minimize the surface decomposition, it has been claimed that an overpressure of AsH$_3$ is necessary for obtaining high-quality epilayers. For atmospheric-pressure MOCVD, it was found that at 650°C the optimum V/III ratio is greater than 30 [32]. It is believed that the surface degradation comes from the As desorption from the grown surfaces and thus raising V/III ratio by increasing AsH$_3$ flow rates should be of help to recover the surface desorption. Fig. 4-3 shows the PL spectra of InGaAs epilayers grown at 650 ~ 685°C with V/III ratios of 130. Clearly, the peak PL intensity for InGaAs grown with V/III ratio of 130 is much stronger than that grown with V/III ratio of 45, both grown at 675°C (Fig. 4-1). Even when the growth temperature is raised to 680°C, the PL intensity is still comparable to those

50

grown at lower temperature. Besides, the improved surface morphology also indicates the impact of V/III ratio on the InGaAs epitaxial materials. Fig. 4-4 shows the relation between the growth temperature and the peak PL intensity of InGaAs epilayers grown with two V/III ratios of 45 and 130. Obviously, the difference of peak PL values for two V/III ratios is smaller at low growth temperature ($<650^{\circ}$C) than that at high temperature ($> 670^{\circ}$C). As the temperature increases further, the influence of V/III ratio is more pronounced and extremely large V/III ratios are suggested to be used. In order to reduce the impurity concentration in the grown epilayers, the temperature should be high. With high V/III ratio (or large AsH$_3$ flow), the maximum of the growth-temperature window can be extended from 650 to 675°C without any compromise with the surface degradation.
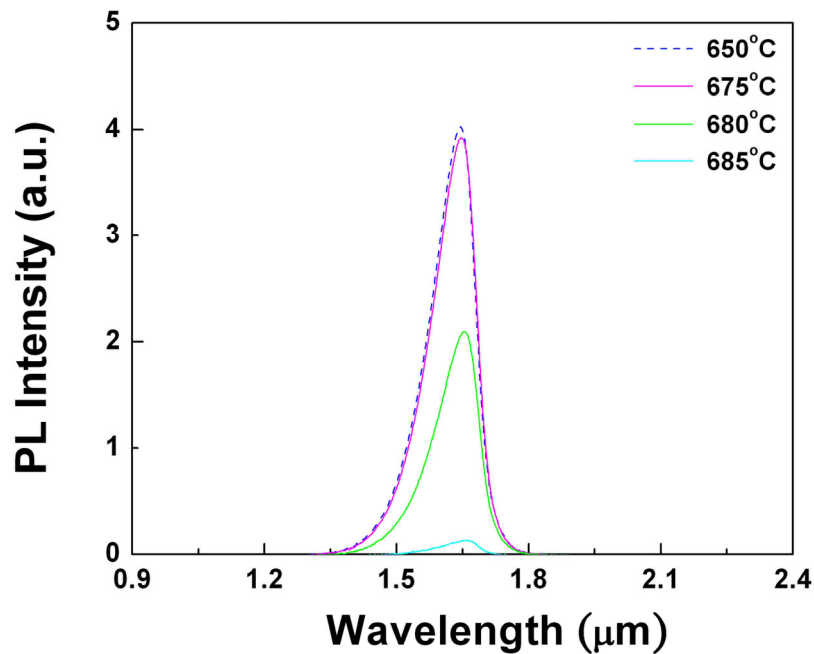
Fig. 4-3:   PL Spectra of InGaAs epilayers grown at 650, 675, 680, and 685°C with V/III~130.
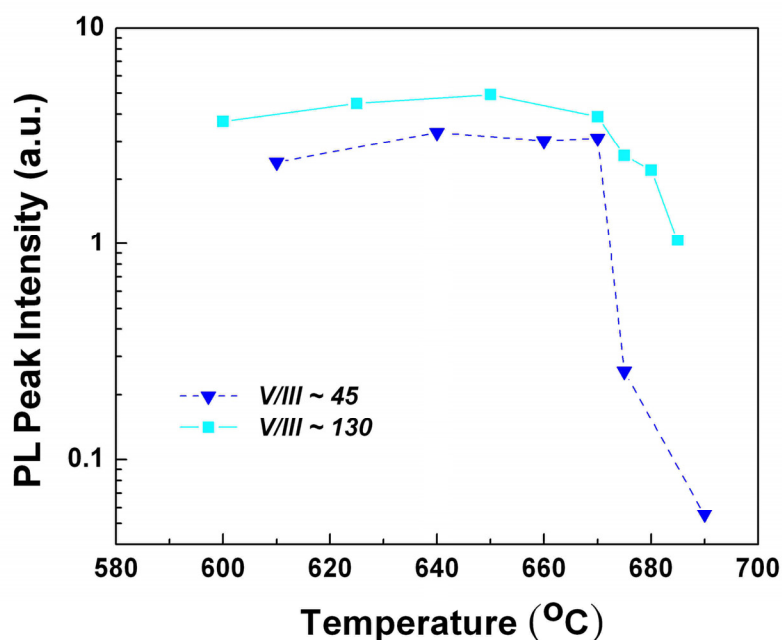
Fig. 4-4: Peak PL intensity of InGaAs epilayers vs. growth temperature with two V/III ratios 45 and 130.

In Fig. 4-4, the correlation between PL peak intensities of InGaAs epilayers and growth temperature has been established. By increasing the V/III ratio, the material quality can be maintained at higher temperatures with the reduction of the impurities. But how far can we increase the V/III ratio to get good-quality InGaAs? To investigate the effects of V/III ratio, several InGaAs epilayers were grown at three temperatures 650, 660, and 675°C, by different V/III ratios (Fig. 4-5). At 650°C, the PL peak value increases as the V/III ratio increases from 25 to 50, beyond which the PL signal saturates. This is because at the low temperature, the degree of As desorption is smooth and there is no need to supply too much overpressure of AsH$_3$ to compensate for loss. If the growth temperature is increased to 660 and 675°C, the impact of the V/III ratio becomes significant. At higher temperature, the amount of

52

group V vacancies from As desorption increases greatly, degrading the epilayers. As a result, to obtain equivalently good epilayers, higher AsH_3 flow rates are required. Though the high V/III ratio can reduce the As loss from the surface when InGaAs is grown at high temperature, there still exists an upper limit for growth temperature. From Fig. 4-5, InGaAs grown at 675^oC of the V/III ratio 130 does not have as high PL peak intensity as those grown at 650^oC with much lower V/III ratio (~25). However, for obtaining high-quality superlattices with fewer impurities, the PL intensity at 675^oC is still acceptable and thus accepted maximum temperature can be extended to 675^oC without any surface degradation.
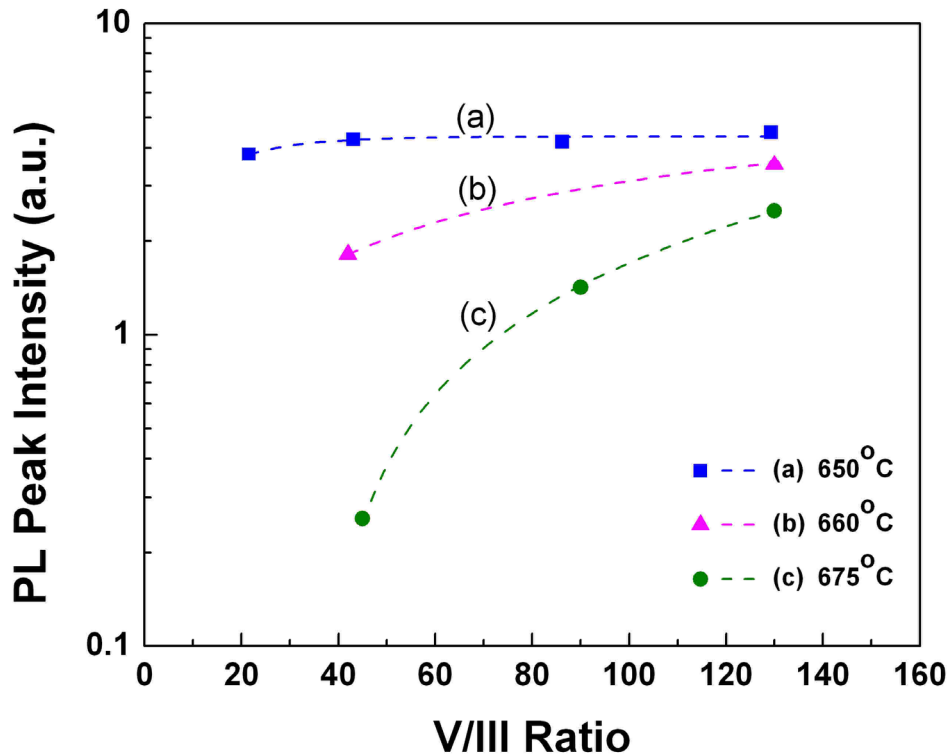
Fig. 4-5:   Peak PL intensity of InGaAs epilayers grown at 650, 660 and 675^oC vs. V/III ratio.

4.1.2 Impacts of Growth Rate

The growth rate, which is believed to be one of the advantages of MOCVD over MBE, has been thought to affect the quality of epilayers [33] significantly. In this thesis, as we increased the growth temperature from 650 to 675°C to extend the maximum temperature, we found that InGaAs epilayers without surface decomposition were not achieved until we increased the growth rate from 4 to 6 Å/s.
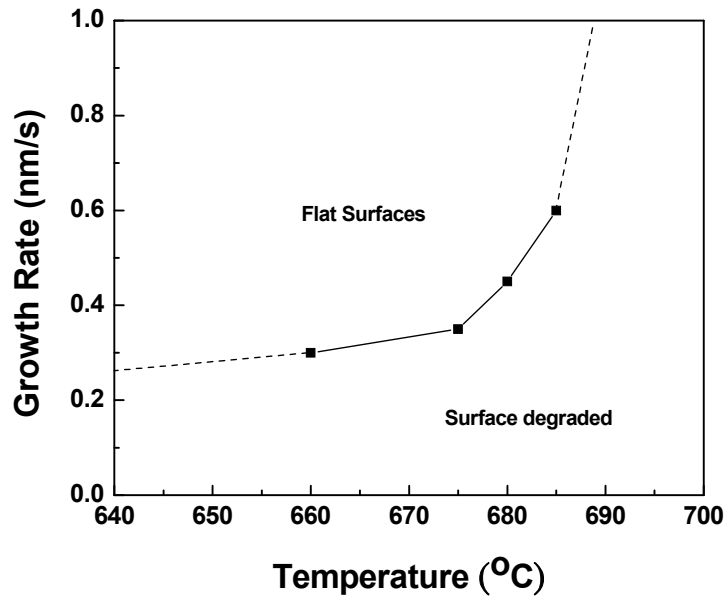
Fig. 4-6: Dependence of the surface decomposition of InGaAs on the growth rate and temperature with V/III ratio ~ 150.

Fig. 4-6 shows the dependence of the grown epilayers without surface degradation on the growth rate and temperature. As the temperature increases, the growth rate needs to be increased as well to avoid the surface decomposition. This may be due to two effects: group V (As) desorption and group III (Ga) desorption.

The former can be remedied by supplying an over-pressure of As atoms and in this study, high V/III ratios were used to reduce this effect as much as possible. From Fig. 4-5, it is clear that with high V/III ratios (above 150) the PL intensity at high growth temperature is still slightly weaker than for a low growth temperature, which hints at another loss mechanism. As the growth temperature increases to 675°C, Ga atoms were desorbed from the grown surface [34]. With higher flow rate of TMG, more Ga atoms are supplied to the growth front, thus reducing the In desorption. Furthermore, the surplus of TMG can also increase the possibility for As atoms to be bonded by them, reducing the surface degradation. So far, with higher growth rate we can grow high-quality InGaAs epilayers without surface decomposition at 690°C which is equal to the highest growth temperature without surface decomposition [9]. Despite the reduction of impurities by increasing growth temperature, the required high growth rate will be problematic for growing high-quality InGaAs/InAlAs superlattices. After discussion of InAlAs epilayers in next section, the solution to this problem will be proposed and the maximum temperature for obtaining high-quality superlattices can be extended to 675°C.

4.2   Optimization of InAlAs Epilayers

Unlike InGaAs, InAlAs, because of the presence of Al content, is found to have poor crystalline and optical properties. Moreover, phase separation and spinodal decomposition occur for InAlAs growth [35]. Due to the large difference of the bond strength of Al-As and In-As, phase separation almost occurs at all temperature [36]. In addition, even with the growth temperature much lower than the critical

temperature T_c, above which no immiscibility gap exists, the spinodal decomposition begins by forming areas with fluctuating compositions slightly different than the grown bulk materials [37]. Moreover, the alloy clustering effect, presumably resulting from the large difference in In-As and Al-As bond energies, also degrades the crystalline quality [38]. As a result, in order to grow high-quality InGaAs/InAlAs superlattices for quantum cascade lasers, a detailed study of InAlAs epilayers is necessary and in this section, we investigate their structural properties by X-ray rocking curves. Combined with the surface morphology obtained by high-resolution optical microscopy, the growth parameters for achieving high-quality InAlAs epilayers can be determined. Following the discussion of InGaAs in the last section, a window of growth parameters for obtaining both InGaAs and InAlAs with good-quality is predicted. In the next section, we will then focus on the optical properties of InGaAs/InAlAs superlattices. With optimized growth parameters, quantum cascade laser growth was attempted and the preliminary results will be discussed in Chapter 5.

Due to its bonding nature and the Al-content, the quality of InAlAs strongly depends on growth conditions such as growth temperature and V/III ratio. The former is especially important because high-temperature growth has been demonstrated to improve the Al-rich alloys [39]. Therefore, we focus on the temperature effect on the structural properties of InAlAs first and then the effect of surface kinetics by adjusting the V/III ratio.

Due to the high concentration of oxygen present at low temperatures, no band-edge emission was observed at temperature below 630°C with low V/III ratio 135 [40]. We will concentrate on growth temperature above 630°C, and thanks to the

conclusion we have about the InGaAs, the maximum temperature for growing high-quality InGaAs/InAlAs superlattices will be lower than 685°C to avoid the surface degradation of InGaAs. Figure 4-7 shows the X-ray linewidth and relative intensity of InAlAs epilayers grown at three growth temperatures 630, 660, and 680°C. The growth parameters are as follows: growth rate ~ 6 Å/s, the reactor pressure 76 torr, the thickness 3500 Å, and the V/III ratio 143 with strain smaller than
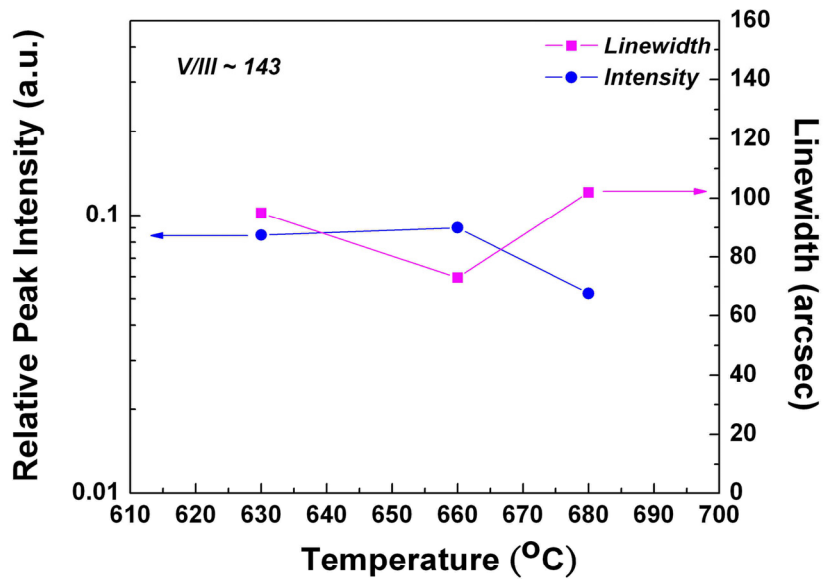
Fig. 4-7:   X-ray linewidth and relative peak intensity of InAlAs epilayers vs. growth temperature.

2×10^{-3}. As the growth temperature increases from 630 to 660°C, the crystal quality is improved with an enhanced peak intensity and reduced linewidth (Fig. 4-7). This is expected due to the fewer impurities incorporated into the epilayers and the enhanced surface mobility of Al atoms (i.e., migration length is larger and thus, extending the

alloy composition fluctuation to a larger scale). Therefore, a higher growth temperature is expected to be suitable for high-quality InAlAs. However, as the temperature increases to 680°C, the X-ray curve became broadened with weaker peak intensity in spite of lower oxygen concentration and higher Al surface mobility which benefit from higher growth temperature. This behavior can be understood as follows: despite the enhanced mobility of Al atoms, the accompanying surface desorption of In will be enhanced with increased temperature, which in turn degrades the crystal quality slightly.
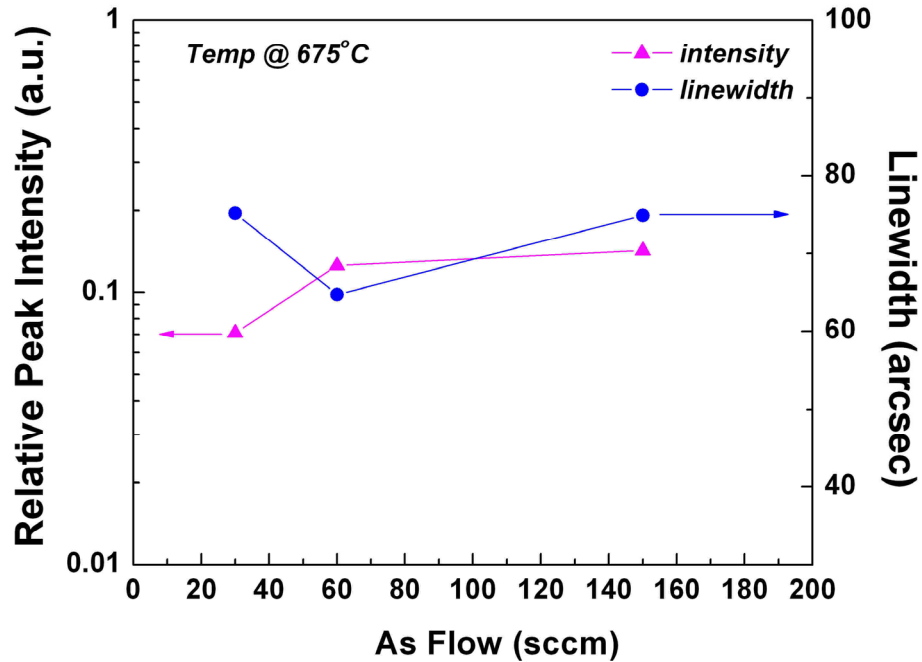
Fig. 4-8: X-ray linewidth and relative peak intensity of InAlAs epilayers vs. AsH₃ flow rate.

From the above discussion, it is demonstrated that the quality of InAlAs strongly correlates with the growth temperature. While the growth temperature of InAlAs epilayers is suggested to be higher than 630°C to reduce impurities, the

maximum growth temperature seems limited to about 680°C, corresponding to the highest growth temperature of InGaAs with reasonable growth rates (~ 6 Å/s) for growing quantum cascade structures (see 4-1-2 and 4-3). The next thing is to determine the effect of V/III ratio on the epilayer quality. To prevent As desorption, we kept the growth temperature at 675°C with other growth parameters unchanged. The flow rate of AsH_3 was adjusted to change the V/III ratio and the grown thickness is 3000 Å with strain smaller than 6×10^{-4}. The results are shown in Fig. 4-8, in which to improve the crystal quality there exists a range for the V/III ratio. This can be explained by the surface kinetics of InAlAs epilayers [19]. If the V/III ratio is too low, the As desorption will be enhanced and due to the large difference of bond strength between In-As and Al-As, most As atoms tend to combine with Al atoms. The As desorption generates more defects and the large difference of bonding strength between In-As and Al-As also causes the alloy fluctuation more pronounced, both contributing to the degraded structural properties. When we increase the V/III ratio, both effects will be reduced and the crystal quality will be improved due to the decreased As-related vacancies and more As atoms bonded to In atoms, eliminating the spinodal decomposition and alloy clustering. In addition, high As overpressure also helps to suppress the surface In desorption at high growth temperatures. However, too much As overpressure will prohibit the Al atoms to move to their sites before the arrival of subsequent Al atoms, degrading the uniformity of alloy composition [19]. As a consequence, unlike InGaAs requiring as high V/III ratio as possible, there exists a range of V/III ratio to obtain high-quality InAlAs epilayers.

Fig. 4-9: Optical image of InAlAs grown at 640°C with V/III ratio 50.

The surface morphology of InAlAs epilayers which are almost lattice-mismatched to InP substrates provides another evidence for material growers to quickly confirm their quality in addition from X-ray rocking curves. At growth temperature below 650°C, the surface morphology exhibits no features with V/III ratio at 50 (in Fig. 4-9). To reduce impurities, the surface morphology of InAlAs grown at higher temperature 675°C was observed with V/III ratios changed from 30 to 150 in Fig. 4-10 (a) – (e). The best morphology with a smooth and flat surface was achieved with V/III ratios below 125. This is because the high growth temperatures enhance the surface mobility of Al atoms and thus improving the quality of InAlAs epilayers. By providing enough As overpressure (in this case V/III ratio > 25), the effect of As desorption and alloy clustering can be reduced to some extent. As V/III ratio increases (> 130), the migration ability of Al atoms is prohibited and the crystal quality thus degrades.
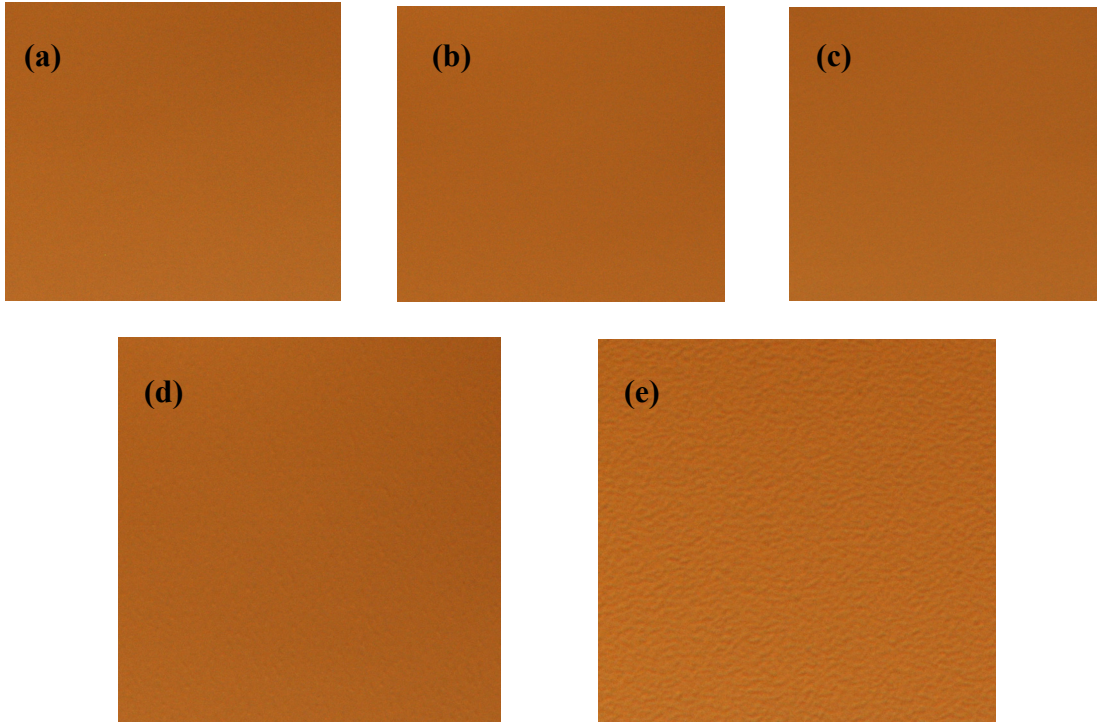
Fig. 4-10: Optical image of InAlAs grown at 675°C with V/III ratio of (a) 30, (b) 59, (c) 88, (d) 116, (e) 149.

In addition to the growth parameters such as temperature and V/III ratio, the surface morphology of InAlAs epilayers could also be improved by growing a buffer layer such as InP and InGaAs epilayers, or short-period superlattices. Therefore, we grew two InAlAs epilayers at 675°C with V/III ratio 143. One is directly grown on the InP substrate and the other is grown with a 50 nm InGaAs buffer layer inserted between the InAlAs epilayer and the substrate. Fig. 4-11 shows the optical images of these two samples and clearly, the morphology of InAlAs with a InGaAs buffer layer (a) is better than without a buffer layer (b). This improvement is due to the smooth growth front created by growing InGaAs first, thus enhancing the mobility of atoms on the surface [41]. Besides, the buffer layer can also inhibit the propagation of the defects originating from the substrate into the epilayer. With short-period

superlattices inserted between the InAlAs and the substrates, the morphology was demonstrated to be improved further [41].

The morphology of InAlAs is consistent with the results obtained from X-ray rocking curves. At higher temperature, InAlAs epilayers with good morphology can be obtained with V/III ratios no larger than 150. High-quality crystals can be obtained with the reduction of impurities by controlling the growth temperature and V/III ratio at the same time.
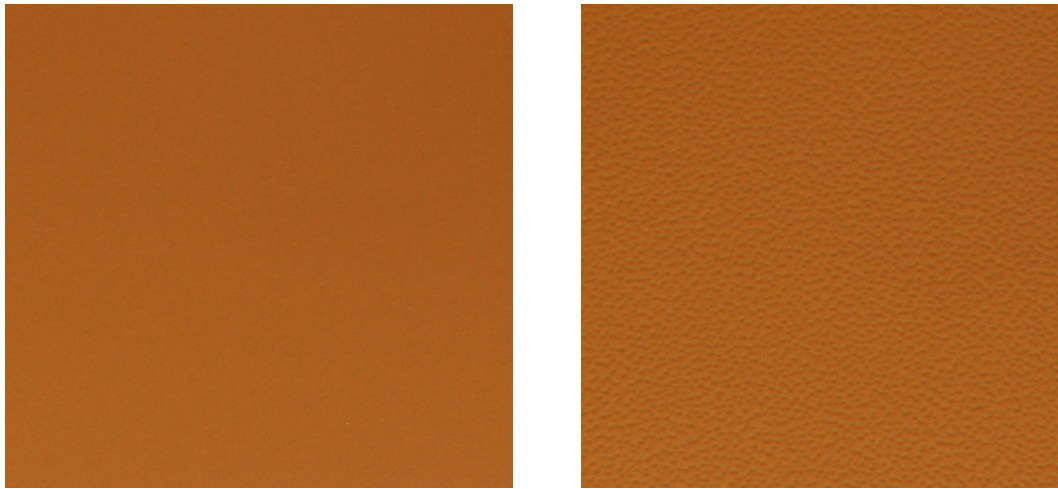
Fig. 4-11: Optical image of InAlAs grown at 675°C: (a) with 50 nm InGaAs buffer layer and (b) directly grown on InP substrate (V/III ratio ~ 145).

4.3   InGaAs/InAlAs Superlattices

Based on the discussion in previous sections, for growing high-quality InGaAs, mid-temperature (640 ~ 660°C) and high V/III ratio should be used to prevent surface decomposition. If we want to increase the growth temperature to further reduce the amount of impurity, then higher growth rates must be used to remedy the surface

decomposition. On the other hand, to achieve high-quality InAlAs epilayers, high temperature is also necessary for eliminating alloy clustering effects. However, the suggested highest V/III ratio to grow InAlAs with good morphology at 675^oC is in contrast, 150, which narrows down the growth window. Besides, lower growth rate, at which InGaAs is unlikely grown without surface decomposition at high growth temperature, was suggested for the growth of Al-containing compound semiconductors [41]. In this section, I will discuss the effect of growth rate, temperature, morphology, and the interruption time between individual layers on the optical properties of InGaAs/InAlAs superlattices. By increasing the interruption period, it is suggested that the quality of superlattices grown at high temperature with high growth rate is comparable with lower temperature/low growth rate.

	InP cap layer	10 nm
Total ~ 30 periods	$\bullet$ $\bullet$ $\bullet$ $\bullet$	
Unit structure	$In_{0.52}Al_{0.48}As$ barrier	10 nm
	$In_{0.53}Ga_{0.47}As$ well	3.2 nm
	$In_{0.52}Al_{0.48}As$ barrier	2.0 nm
	$In_{0.53}Ga_{0.47}As$ well	2.2 nm
	$In_{0.52}Al_{0.48}As$ barrier	50 nm
	$In_{0.53}Ga_{0.47}As$ buffer layer	50 nm
	InP substrate	
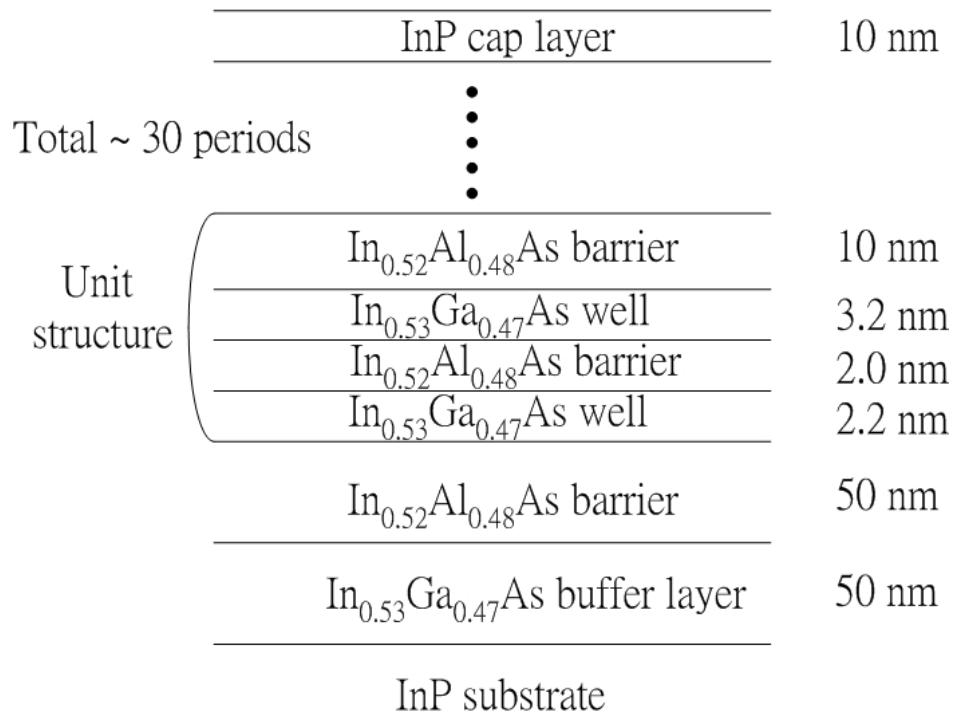
Fig. 4-12: Superlattice structure

63
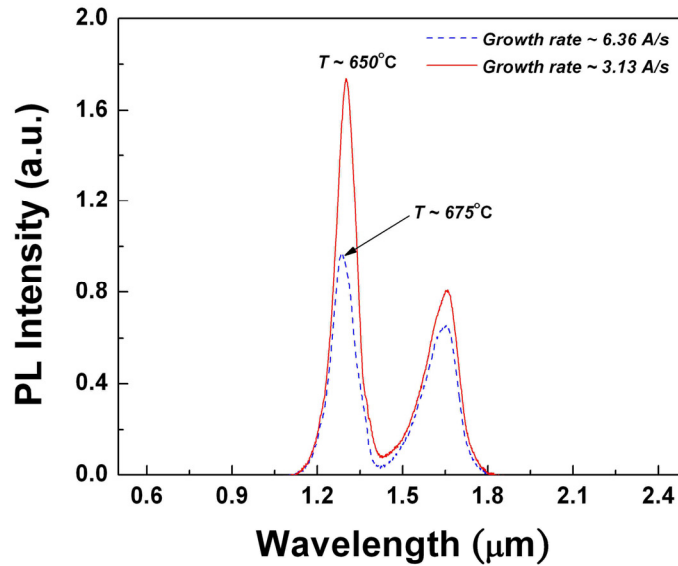
Fig. 4-13: PL spectra of superlattices with different growth temperatures and growth rates.

The superlattices structure has 30 repeated units and each is comprised of four layers: 10 nm InAlAs/3.2 nm InGaAs/2nm InAlAs/2.2 nm InGaAs (Fig. 4-12). Before these layers were grown, a 50 nm InGaAs buffer layer was deposited and then a 50 nm InAlAs cladding layer. Finally, the superlattices were covered with a thin capping InP layer. Fig. 4-13 shows the room-temperature PL spectra of the superlattices grown at 650°C with 3 Å/s and at 675°C with 6 Å/s (V/III ratio above 130). There are two peaks in these PL spectra at 1.3 μ m and 1.65 μ m, which correspond to the emissions from the quantum confinement in superlattices and from the InGaAs buffer layers. The peak value of at 1.3 μ m emission from the superlattices is higher at the growth temperature 650°C with lower growth rate. This can be explained as follows: first, InGaAs of superlattices grown at 650°C is of better quality than those grown at 675°C due to lower desorption (see Fig. 4-5). Secondly, a
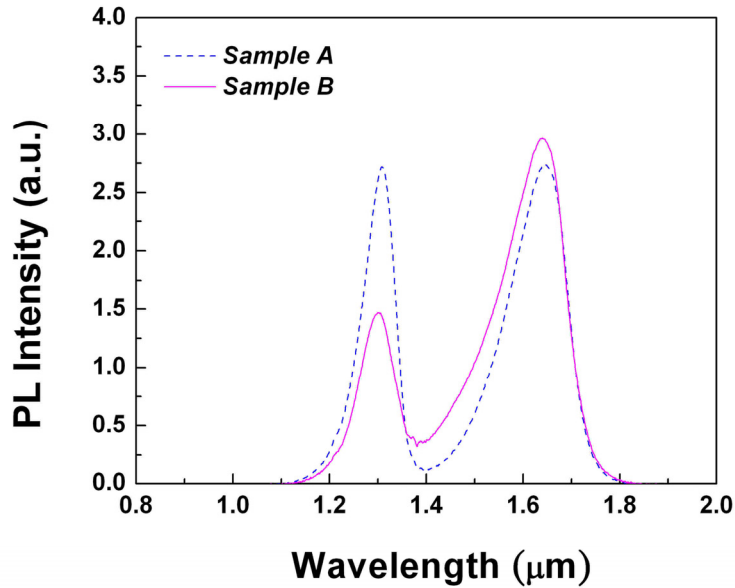
Fig. 4-14:   PL spectra of superlattices of two different level of surface morphology of InAlAs, sample A is flat and sample B is bad.

lower growth rate also allows Al atoms more time to move to their sites before the subsequent atoms arrive [33]. However, the surface morphology of InAlAs epilayers grown at 650°C was poor due to the high V/III ratio, which inhibits the Al surface mobility. If the surface is worse, the surface scattering will be enhanced, raising the possibilities for non-radiative emission. As a result, we expect InAlAs epilayers with better morphology can improve the optical properties of superlattices. To explore this effect, we grew two superlattices A and B at the same temperature except for different V/III ratios for growing InAlAs by keeping the growth condition of InGaAs unchanged. The morphology of InAlAs of sample A is perfectly flat but for B, it's poor. The influence of surface morphology of InAlAs on the superlattices can be seen from Fig. 4-14, in which the intensity of sample A is stronger than that of sample B.

By adjusting V/III ratio (mentioned in last section), the surface morphology of InAlAs can be improved with reduced scattering from the rough surface.
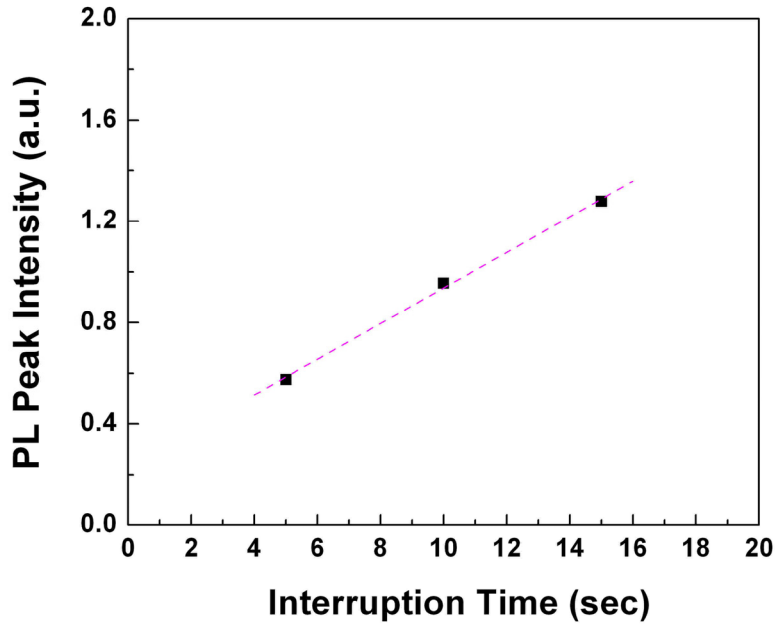
Fig. 4-15:   PL peak intensity vs. the interruption time.

As discussed in 4.1.2, while increasing temperature can reduce the impurities, the critical growth rate below which the surface decomposition occurs increases. However, the crystal quality and the interfaces between InGaAs and InAlAs layers become worse as the growth rate increases. To solve this problem, a growth interruption (purge) between InGaAs and InAlAs is suggested to recover the quantum confinement effects by room-temperature photoreflectance measurement [42]. We studied the effect of interruption time on the superlattice quality by room-temperature PL with different growth interruption times 5s, 10, 15s, and 25s. The interruption was between the time that the group III sources for InGaAs (TMI and TMG) are turned

off and the time that the sources for InAlAs (TMI and TMA) are turned on with only AsH$_3$ purging, and vice versa. With the interruption, the surface quality between InGaAs and InAlAs layers can be improved with sharper interfaces because the adatoms have more time to migrate to their sites. Besides, the inter-diffusion between the constituents in InGaAs and InAlAs can be decreased to preserve the designed quantum levels within the conduction band, which is very important for quantum cascade lasers. Fig. 4-15 shows the peak PL intensity of superlattices versus interruption time. As the time increases from 5 s to 15 s, the intensity also increases correspondingly, which means the interface quality is improved with growth interruption. However, once the growth interruption increases to 25s, the PL intensity is reduced by a factor of four, indicating the interruption favors the incorporation of non-radiative impurities at the interface when the growth interruption time exceeds 15 s.

In addition to the study of interruption, we also grew a sample without purging by switching the TMG and TMA lines and without turning off the TMI and AsH$_3$ flows. The PL intensity is strongest for all superlattices grown with any interruption and the emission wavelength was shifted to shorter wavelength ~ 1.245 μ m. The wavelength shift is due to the formation of InGaAlAs quaternary layers from the residual flows during switching processes [43]. Since the switching only involves the Ga and Al flows, the material is always lattice matched and the material quality is the highest of all grown samples without impurities incorporated during the interruption period.

With interruption at the interface, the roughness of superlattices grown at 675°C with high growth rate (6 Å/s) can be reduced to be comparable with that grown at 650°C with a low growth rate (3 Å/s). Higher growth temperature can be used to reduce the impurities incorporated into the interfaces with interruption time between individual layers. With the high grow rate required at high growth temperature, the interface quality can be improved by using a long interruption period. The maximum growth temperature for growing InGaAs/InAlAs superlattices is extended to 675°C, higher than the temperature 650°C that has been generally thought to be the optimized temperature [44]. In this study, the growth temperature was successfully extended from 650 to 675°C with higher growth rate and, by long interruption time (~ 15s) a wider window for growing high-quality superlattices with comparable performance was obtained.

Chapter 5

Material Growth of Quantum Cascade Lasers and Future Plans

5.1   Short-Wavelength Quantum Cascade Lasers

In Chapter 4, the growth conditions of InGaAs and InAlAs and the InGaAs/InAlAs superlattices were investigated. We concluded that to reduce the impurities, the temperature needs to be increased, but at the same time an upper limit exists to avoid the surface degradation of InGaAs. By increasing the growth rate to 6 Å/s (Fig. 4-6), the maximum growth temperature can be raised to 675°C without weakening their PL intensities. On the other hand, high-quality InAlAs epilayers can also be grown at 675°C with V/III ratio smaller than 150 for flat grown surfaces. Therefore, we set the substrate temperature at 675°C with V/III ratio 100 ~ 150 to grow the quantum cascade structures. Our target is to grow shorter-wavelength QCLs (3 ~ 5 μ m) and the preliminary results provide a strong evidence to grow high-quality materials.

Typically, there are three major categories of the short wavelength QCLs requires: (a) Strained-balanced InGaAs/InAlAs [45]; (b) InAs/AlSb/GaSb [46]; (c) InGaAs/AlAsSb [47]. The first system has been demonstrated with high performance, but there exists a compromise between the emission wavelength and their lattice match conditions. Though the second system provides enough conduction band offset to emit NIR photons, the substrate used is GaSb whose material growth tecchnique is much less developed compared to InP and GaAs technology, causing more problems
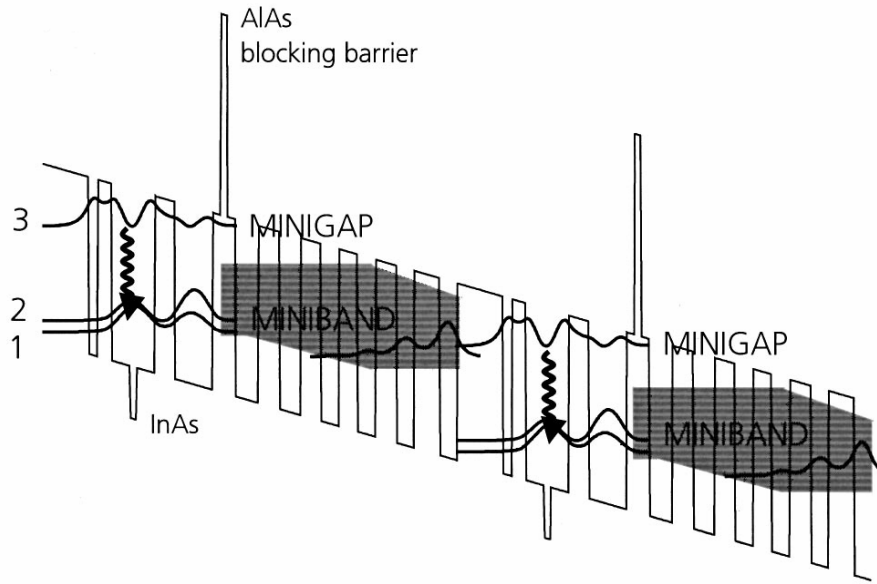
Fig. 5-1:   Quantum cascade structure with InAs and AlAs inserted into InGaAs/InAlAs to improve the efficiency and extend the emission wavelength to below 5 μ m [48].

such as its higher resistance and carrier loss, and poorer thermal conduction. The last system is promising because of the large difference of conduction band energy between InGaAs and AlAsSb. However, the immaturity of the growth of Sb-containing alloys by MOCVD is a fundamental problem from material aspects. As a result, a new scheme utilizing an InAs/AlAs binary compound semiconductors inserted into typical InGaAs/InAlAs superlattices is a candidate for obtaining NIR QCLs [48] by MOCVD (Fig. 5-1). Though the operation temperature for this type QCLs is still below room temperature, from the viewpoint of material growth, this structure is much easier to grow and to characterize. By X-ray diffraction, useful information can be extracted such as the periodicity and lattice mismatch condition.

Because of the large difference of the lattice constants of InAs and AlAs with $In_{0.53}Ga_{0.47}As$ and $In_{0.52}Al_{0.48}As$ (lattice-matched to InP substrate), the lattice

70

mismatch condition requires special attention to prevent the large strains for growing

thick layers ($\sim 2\,\mu$m, for QCLs). We grew a superlattice modified from the structure

in Chapter 4 with the insertion of 5Å InAs and 6.5Å AlAs into the well and barrier

regions to test the lattice match condition, growth rates of InAs and AlAs, and its

periodicity (Fig. 5-2). The result is shown in Fig. 5-3. The net strain is extremely

small ($\sim 3.5\times10^{-4}$) and the period was calculated based on the discussion in Chapter 3

to be 192 Å, which is close to the designed value (186 Å) with 3.2 % error. From this

Fig. 5-2: Modified superlattice structure with the insertion of InAs and AlAs digital alloys.

X-ray rocking curve, we clearly observed several satellite peaks (-4 to +4), indicating the uniformity of the superlattice periodicity. The intensity and the linewidths of satellite peaks provide further evidence for the quality of the superlattice. Because of the extremely large lattice mismatch between InAs (or AlAs) and InP, it is difficult to calibrate the growth rate by growing a thick InAs or AlAs epilayer on InP. From X-ray rocking curves, the period can be calculated and once we know the growth rates of InGaAs and InAlAs, we can easily calibrate the growth rates of InAs and AlAs.
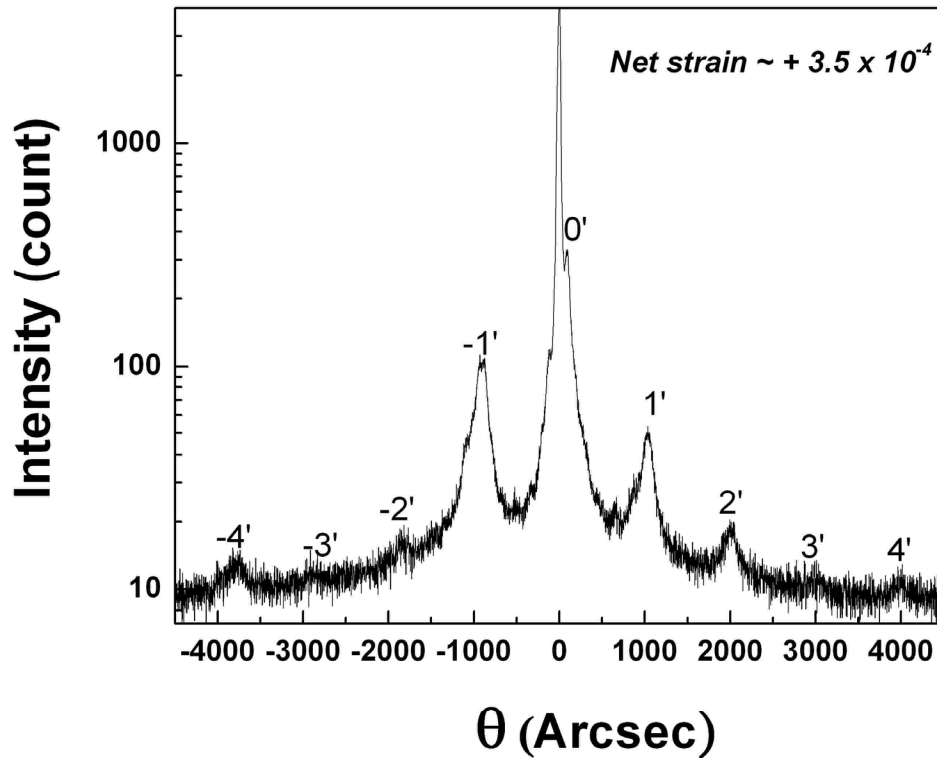
Fig. 5-3: X-ray rocking curve of InGaAs/InAlAs superlattice with InAs and AlAs insertion layers.

5.2 Future Plans

So far, I have investigated the material aspects of InGaAs and InAlAs, the basic units for QCLs. A narrow window of the growth parameters for achieving high-quality InGaAs and InAlAs at the same time was obtained by exploring the effect of the growth rates, growth temperature, and the V/III ratios. InGaAs/InAlAs superlattices lattice-matched to InP substrate were grown and by adding an interruption time between individual layer growth, the performance of superlattices grown at high temperatures with high growth rates can be improved. To extend the emission wavelength of QCLs to shorter wavelength, several methods have been proposed and have demonstrated their advantages and disadvantages. The InGaAs/InAlAs lattice-matched system with InAs/AlAs digital-alloys insertion is promising for MOCVD growth, and we have successfully grown superlattices with InAs/AlAs with high crystal quality and good periodicity, which is very important for QCLs. Before we start to grow the whole QCL structure of digital alloys, several $8\,\mu$m QCLs with lattice-matched InGaAs/InAlAs were grown successfully and are now in the device processing stage.

This thesis is pioneering in its efforts to study the high-temperature growth of InGaAs/InAlAs superlattices, optimization of the growth parameters and also short-wavelength QCLs. Further work is still required to investigate the following issues:

1. The electrical properties of InGaAs and InAlAs: Because we only characterized InGaAs and InAlAs from their optical and structural properties, and the surface morphology, lack of information about carrier mobility hinders our further

understanding about the effect of the carrier transport on the QCL performance. If the information about carrier mobility is acquired, combined with the optical properties that we have obtained, the in-depth relationship between the QCL performance and the growth parameters can be established.

2. Optimization of growth rates and temperature: Though we have successfully grown high-temperature superlattices with high growth rate, it is still not clear whether the high-temperature with high growth rate will be the optimized condition for growing QCLs. Based on the results in Chapter 4 the superlattice grown at 650°C with a low growth rate has a stronger PL intensity compared to 675°C with higher growth rate. There may exist a optimized condition between these two temperatures, requiring further investigation.

3. Effects of InAs and AlAs digital alloys: With InAs/AlAs insertion, structural information was obtained, but no information about the effects from the extra heterointerfaces between InAs/InGaAs and AlAs/InAlAs was obtained. The comparison between this digital alloy scheme and the strained-balanced InGaAs/InAlAs must be done to understand the effects of InAs/AlAs on the optical properties of superlattices before we grow QCLs.

Bibliography

[1] R. F. Kazarinov and R. A. Suris, "Possibility of the amplification of electromagnetic waves in a semiconductor with a superlattice," *Soviet Physics Semiconductors*, vol. 5, no. 4, pp. 707–709, 1971.

[2] J. Faist *et al*., "Quantum cascade lasers," *Science*, vol. 264, pp. 553–556, 1994.

[3] J. S. Yu *et al*., "High-power continuous-wave operation of quantum-cascade lasers up to 60$^\mathrm{o}$C," *IEEE Photonics Technology Letters*, vol. 16, no. 3, pp. 747–749, 2004.

[4] C. Gmachl *et al*., "Dependence of the device performance on the number of states in quantum-cascade lasers," *IEEE Journal of Selected Topics in Quantum Electronics*, vol. 5, no. 3, pp. 808–816, 1999.

[5] F. Capasso et al., "New frontier in quantum cascade lasers and applications," *IEEE Journal of Selected Topics in Quantum Electronics*, vol. 6, no. 6, pp. 931–947, 2000.

[6] C. Gmachl, F. Capasso, D. L. Sivco, and A. Y. Cho, "Recent progress in quantum cascade lasers and applications," *Report on Progress in Physics*, vol. 64, pp. 1533–1601, 2001.

[7] C. Walther, G. Scalari, J. Faist, H. Beere, and D. Ritchie, "Low frequency terahertz quantum cascade lasers operating from 1.6 to 1.8 THz," *Applied Physics Letters*, vol. 89, pp. 231121, 2006.

[8] D. G. Revin *et al*., "InGaAs/AlAsSb/InP quantum cascade lasers operating at wavelengths close to 3 μm," *Applied Physics Letters*, vol. 90, pp. 021108, 2007.

[9] Green R. *et al.*, "MOVPE grown quantum cascade lasers," *Physica E*, vol. 21, pp. 863–866, 2004.

[10] Liu Z. *et al.*, "Room-temperature continuous-wave quantum cascade lasers grown by MOCVD without lateral regrowth," *IEEE Photonics Technology Letters*, vol. 18, no. 12, pp. 1347–1349, 2006.

[11] L. Diehl et al., "High-temperature continuous wave operation of strain-balanced quantum cascade lasers grown by metal organic vapor-phase epitaxy," *Applied Physics Letters*, vol. 89, pp. 081101, 2006.

[12] H. I. Schiff, G. I. Mackay, and J. Bechara, *Air Monitoring by Spectroscopic Techniques*, editor M. W. Sigrist, New York: Wiley-Interscience, 1994.

[13] J. Faist et al., "Distributed feedback quantum cascade lasers," *Applied Physics Letters*, vol. 70, no. 20, pp. 2670–2672, 1997.

[14] J. H. Shorter et al., "Measurement of nitrogen dioxide in cigarette smoke using quantum cascade tunable infrared laser differential absorption spectroscopy (TILDAS)," *Spectrochimica Acta Part A-Molecular and Biomolecular Spectroscopy*, vol. 63, pp. 994–1001, 2006.

[15] Q. K. Yang, C. Mann, F. Fuchs, K. Kohler, W. Bronner, "High-temperature (T $\geq$ 400K) operation quantum cascade lasers with thin InAs of strain-compensated insertion layers and AlAs blocking barriers," *Journal of Crystal Growth*, vol. 278, pp. 714–717, 2005.

[16] T. Soga, Y. Takahashi, S. Sakai, and M. Umeno, "High-temperature growth-rate in MOCVD growth of AlGaAs," *Journal of Crystal Growth*, vol. 68, pp. 169–175, 1984.

[17] Herman M. A., Richter W., and Sitter H., *Epitaxy: Physical Principles and Technical Implementation*, Berlin, Germany: Springer, 2004.

[18] Venables J. A., "Nucleation and growth of thin films," *Reports on Progress in Physics*, vol. 47, pp. 399–459, 1984.

[19] Welch D. F., Wicks G. W., Eastman L. F., Parayanthal P., and Pollak F. H., "Improvement of optical characteristics of $Al_{0.48}In_{0.52}As$ grown by molecular beam epitaxy," *Applied Physics Letters*, vol. 46, no. 2, pp. 169–171, 1985.

[20] H. Ito and H. Yokoyama, "Carbon doping in InAlAs grown by metalorganic chemical vapor deposition," *Journal of Crystal Growth*, vol. 173, pp. 315–320, 1997.

[21] S. R. Andrews and B. A. Miller, "Experimental and theoretical-studies of the performance of quantum-well infrared photodetectors," *Journal of Applied Physics*, vol. 70, no. 2, pp. 993–1003, 1991.

[22] V. Swaminathan and A. T. Macrander, *Materials Aspects of GaAs and InP Based Structures*, Englewood Cliffs, New Jersey, Prentice Hall, 1991.

[23] G. Bauer and W. Richter, *Optical Characterization of Epitaxial Semiconductor Layers*, Germany, Springer-Verlag, 1996.

[24] V. S. Speriosu and T. Vreeland, "X-ray rocking curve analysis of superlattices," *Journal of Applied Physics*, vol. 56, no. 6, pp. 1591–1600, 1984.

[25] G. B. Stringfellow, *Organometallic Vapor-Phase Epitaxy: Theory and Practice*, Academic Press, 1999.

[26] R. Bhat *et al.*, "Growth of high quality AlInAs by low pressure organometallic chemical vapor deposition for high speed and optoelectronic device

applications," *Journal of Crystal Growth*, vol. 108, pp. 441–448, 1991.

[27] J. I. Davis, P. D. Hodson, A. C. Marshall, M. D. Scott, and R. J. M. Griffiths, "Improvements in the structural quality of $Al_{0.48}In_{0.52}As$ grown by low pressure metal-organice vapour-phase epitaxy," *Semiconductor Science and Technology*, vol. 3, pp. 223–226, 1988.

[28] J. te Nijenhuis, P. R. Hageman, and L. J. Giling, "Dependence of indium incorporation upon the substrate misorientation during growth of $In_xGa_{1-x}As$ by metalorganic vapour phase epitaxy," *Journal of Crystal Growth*, vol. 167, pp. 397–405, 1996.

[29] J. Hellara, K. Borgi, H. Maaref, V. Souliere, and Y. Monteil, "Optical properties of InP/InAlAs/InP grown by MOCVD on (100) substrates: influence of V/III molar ratio," *Materials Science and Engineering C*, vol. 21, pp. 231–236, 2002.

[30] S. J. Bass *et al*., "Effect of growth temperature on the optical, electrical and crystallorgraphic properties of epitaxially indium gallium arsenide grown by MOCVD in an atmospheric pressure reactor," *Journal of Crystal Growth*, vol. 79, pp. 378–385, 1986.

[31] K. L. Fry, C. P. Kuo, R. M. Cohen, and G. B. Stringfellow, "Photoluminescence of organometallic vapor phase epitaxial GaInAs," *Applied Physics Letters*, vol. 46, pp. 955–957, 1985.

[32] C. P. Kuo, R. M. Cohen, K. L. Fry, and G. B. Stringfellow, "Characterization of $Ga_xIn_{1-x}As$ grown with TMI," *Journal of Electronic Materials*, vol. 14, pp. 231–244, 1985.

[33] F. Y. Juang *et al*., "Growth and properties of $In_{0.52}Al_{0.48}As/In_{0.53}Ga_{0.47}As$, GaAs:

In and InGaAs/GaAs multilayers," *Journal of Crystal Growth*, vol. 81, pp. 373–377, 1987.

[34] R. Heckingbottom, "Thermodynamic aspects of molecular beam epitaxy: High temperature growth in the GaAs/Ga1-xAlxAs system," *Journal of Vacuum Science and Technology B*, vol. 3, no. 572–575, 1985.

[35] K. Kurihara et al., "Phase separation in InAlAs grown by MOVPE with a low growth temperature," *Journal of Crystal Growth*, vol. 271, pp. 341–347, 2004.

[36] H. K. Cho et al., "Observation of phase separation and ordering in the InAlAs epilayer grown on InP at the low temperature," *Materials Science and Engineering B*, vol. 64, pp. 174–179, 1999.

[37] G. B. Stringfellow, "Miscibility gaps and spinodal decomposition in III/V quaternary alloys of the type $A_xB_yC_{1-x-y}D$," *Journal of Applied Physics*, vol. 54, pp. 404–409, 1983.

[38] Singh J. and K. K. Bajaj, "Role of interface roughness and alloy disorder in photoluminescence in quantum-well structures," *Journal of Applied Physics*, vol. 57, pp. 5433–5437, 1985.

[39] W. T. Tsang, F. K. Reinhart, and J. A. Ditzenberger, "Very low current threshold GaAs-Al_xGa_{1-x}As double-heterostructure lasers grown by molecular beam epitaxy," *Applied Physics Letters*, vol. 36, pp. 11–14, 1980.

[40] H. Kamei, "Growth of AlInAs and heterostructures on InP by OMVPE," *Journal of Crystal Growth*, vol. 93, pp. 329–335, 1988.

[41] E. Tournié, Y. –H. Zhang, N. J. Pulsford, K. Ploog, "Structural and optical properties of $Al_{0.48}In_{0.52}$As layers grown on InP by molecular beam epitaxy:

Influence of the substrate temperature and of a buffer layer," *Journal of Applied Physics*, vol. 70, pp. 7362–7369, 1991.

[42] W. C. H. Choy *et al.*, "The effect of growth interruption on the properties of InGaAs/InAlAs quantum well structures," *Applied Physics Letters*, vol. 72, pp. 338–340, 1998.

[43] M. C. Y. Chan, Y. Chan, and E. H. Li, "Modeling of optical gain properties of multiple cations InGaAs-InAlAs quantum well intermixing," *IEEE Journal of Quantum Electronics*, vol. 34, no. 3 pp. 519–525, 1998.

[44] D. Pavlidis, K. Hong, K Hein, and Y. Kwon, "Material and device properties of MOCVD grown InAlAs/InGaAs HEMTs," *Solid State Electronics*, vol. 38, no. 9, pp. 1697–1701, 1995.

[45] J. S. Yu *et al.*, "High-power, room-temperature, and continuous-wave operation of distributed-feedback quantum-cascade lasers at $\lambda \sim 4.8 \mu$ m," *Applied Physics Letters*, vol. 87, pp. 041104, 2005.

[46] J. Devenson, D. Barate, R. Teissier, and A. N. Baranov, "Short wavelength (3.5 $\sim 3.65 \mu$ m InAs/AlSb quantum cascade lasers," *Electronics Letters*, vol. 42, pp. 1284–1286, 2006.

[47] D. G. Revin *et al.*, "InGaAs/AlAsSb/InP quantum cascade lasers operating at wavelengths close to 3μ m," *Applied Physics Letters*, vol. 90, pp. 021108, 2007.

[48] Q. K. Yang *et al.*, "Improvement of $\lambda \approx 5 \mu$ m quantum cascade lasers by blocking barriers in the active regions," *Applied Physics Letters*, vol. 80, no. 12, pp. 2048–2050 2002.